Formation and Modification of $MgO{\cdot}Al_2O_3$-Based Inclusions in Alloy Steels

SHUFENG YANG, QIANGQIANG WANG, LIFENG ZHANG, JINGSHE LI, and KENT PEASLEE

The current study performed thermadynamic calculation, laboratory experiments, and industrial trials for the formation and modification of MgO-Al_2O_3 spinel inclusions in alloy steels. The stability Mg-Al-O diagram was obtained using the thermodymanic study. The resulting MgO-Al_2O_3-CaO inclusions from MgO-Al_2O_3 spinel inclusions after the calcium treatment were spherical, and > 5 μm MgO-Al_2O_3-CaO inclusions have a two-layer structure: an outside CaO-Al_2O_3 layer and a MgO-Al_2O_3 core. The modification of > 5 μm $MgO{\cdot}Al_2O_3$ spinel inclusions by calcium treatment includes two steps: (1) reducing MgO in the inclusion into the dissolved magnesium by the dissolved calcium in the steel and (2) generating a liquid $x CaO{\cdot}yAl_2O_3$ layer at the outside of the spinel inclusion. For <2 μm $MgO{\cdot}Al_2O_3$ spinel inclusions, they can possibly be modified into a $x CaO{\cdot}yAl_2O_3$ inclusion by reducing all MgO component in the spinel inclusions with the added calcium.

DOI: 10.1007/s11663-012-9663-1

I. INTRODUCTION

$MgO{\cdot}Al_2O_3$ spinel inclusions are harmful to both the quality of products and the castability of the steel because of their high melting point and high hardness. $MgO{\cdot}Al_2O_3$ spinel inclusions deteriorate the corrosion resistance of the steel and cause surface defects and cracks during deep drawing or spinning manufacturing of the steel. Several investigations have been reported on how spinel inclusions form in the molten steel both thermodynamically and experimentally. For example, Inada and Todoroki[1] found that sliver-like defects appeared on the cold sheet of an Al-killed 430 stainless steel, and Park and Todoroki[2] reported there were swollen defects on a deeply drawn product. Spinel inclusions tend to accumulate on the inner wall of the submerged entry nozzle.[3–10] The clogged inclusions at the submerged entry nozzle may be dislodged into the steel and finally entrapped to the solidified shell and become serous internal defects.

Four mechanisms on the formation of $MgO{\cdot}Al_2O_3$ inclusions were reported: direct reaction model,[11–14] Al-reduction model,[15,16] C-reduction model,[17,18] and Si-reduction model (or crystallization model),[19–21] as summarized in Tables I and II. Only three sources of $MgO{\cdot}Al_2O_3$ spinel inclusions are possible: (1) deoxidizer, (2) ladle slag, (3) ladle lining, (4) tundish slag, and (5) tundish lining. For the deoxidizer, if Al-Mg alloy, which is the most popular Al alloy that contains ~3 pct to 5 pct magnesium, is wrongly used rather than pure aluminum to make the AlFe alloy as the deoxidizer, then magnesium will be dissolved into the molten steel, and subsequently, $MgO{\cdot}Al_2O_3$ inclusions will be generated. However, it is impossible for steelmakers to make this mistake. For ladle slag and tundish slag, MgO is rarely added. Thus, the most possible sources of MgO in the inclusions are ladle lining and tundish lining, especially nowadays, MgO-graphite and MgO-CaO-graphite bricks was extensively used in the lining refractory for ladles and tundishes. For tundish, a layer of coating of lining materials contacts the molten steel either by the spraying process or by the man-made coating process. This layer is far looser and more porous than bricks; thus, it is easier to react with molten steel. So, the tundish lining coating layer is a more serious source of $MgO{\cdot}Al_2O_3$ inclusions than ladle lining refractory.

It was debated whether $MgO{\cdot}Al_2O_3$ spinel inclusions can be effectively modified to liquid ones by calcium treatment. It was reported that the modification of $MgO{\cdot}Al_2O_3$ spinel inclusions by calcium treatment was less effective than the modification of pure alumina because of the smaller activity of alumina in the spinel inclusions.[32] A plant trial shows little modification in both the morphology and composition of $MgO{\cdot}Al_2O_3$ spinel inclusions by calcium treatment during ladle refining, and the authors concluded that this was possible because the spinel phase had a cubic crystal structure and was very stable at a high temperature.[33]

However, more recent work reported that the addition of Ca had a great effect on the stability of $MgO{\cdot}Al_2O_3$ inclusions not only by theoretical analysis but also by practical operations, and the conclusion was that $MgO{\cdot}Al_2O_3$ inclusions can be modified by calcium

SHUFENG YANG, Lecturer, QIANGQIANG WANG, Ph.D. Student, and LIFENG ZHANG and JINGSHE LI, Professors, are with the School of Metallurgical and Ecological Engineering, University of Science and Technology Beijing (USTB), Beijing 100083, P.R. China. Contact e-mail: zhanglifeng@ustb.edu.cn KENT PEASLEE, Professor, is with the Department of Materials Science & Engineering, Missouri University of Science and Technology (Missouri S&T), Rolla, MO 65409-0330.

Manuscript submitted July 6, 2011.
Article published online April 24, 2012.

Table I. Main Reactions for the Formation of $MgO{\cdot}Al_2O_3$ Spinel Inclusions in the Steel

Model	Main Reactions	Reference(s)
C-reduction model	$MgO_{(s)} + C_{(s)} = Mg_{(g)} + CO_{(g)}$ $Mg_{(g)} = [Mg]$ $[Mg] + CO_{(g)} = MgO_{(s)} + [C]$ $2[Al] + 3CO_{(g)} = Al_2O_{3(s)} + 3[C]$ $[Mg] + 4[O] + 2[Al] = MgO{\cdot}Al_2O_{3(s)}$ $3[Mg] + 4Al_2O_{3(s)} = 2[Al] + 3MgO{\cdot}Al_2O_{3(s)}$ $3[Mg] + Al_2O_{3(s)} = 2[Al] + 3MgO$	[17,18]
Direct reaction model	$MgO_{(s)} + Al_2O_{3(s)} = MgO.Al_2O_{3(s)}$ $MgO_{(s)} + 2[Al] + 3[O] = MgO{\cdot}Al_2O_{3(s)}$	[11–14]
Al-reduction model	$3(MgO) + 2[Al] = (Al_2O_3) + 3[Mg]$ $[Mg] + 4/3\ (Al_2O_3) = MgO.Al_2O_3 + 2/3[Al]$	[15,16]
Si-reduction model	$2(MgO)_{slag\ or\ ling} + [Si] = (SiO_2)_{slag\ or\ inclusion} + 2[Mg]$ $[Mg] + [O] = (MgO)_{inclusion}$ $2[Al] + 3[O] = (Al_2O_3)_{inclusion}$ $(MgO) + (Al_2O_3) = MgAl_2O_{4(s)}$	[19–21]

treatment even easier than pure alumina inclusions. Itoh *et al.*[22] found that even a very small amount of Ca could strongly affect the phase boundary between spinel and alumina, and according to his stability phase diagram of the Mg-Al-Ca-O system, 1 ppm Ca in the steel could significantly decrease the stability of spinel inclusions and dramatically increase the stability of liquid $MgO\text{-}Al_2O_3$ inclusions. YoungJo *et al.*[34] studied the formation mechanism of liquid calcium alumina inclusions originating from $MgO\text{-}Al_2O_3$ spinel materials and found that spinels reacted with the dissolved Ca forming a liquid calcium aluminate phase. Pistorius *et al.*[35] suggested that MgO could significantly contribute to liquefy inclusions by calcium treatment, so less calcium was needed when MgO was present in the starting inclusions. They concluded that calcium treatment can successfully modify the spinel inclusions to mixed alumina-lime-magnesia inclusions, and the shapes of inclusion transfer from irregular into globular. They also found that after calcium treatment, the inclusions were inhomogeneous in composition, in which areas richer in Ca were depleted of Mg and *vice versa*. So, they proposed a mechanism of spinel modification by preferential reduction of MgO from the spinel; laboratory and industrial samples were analyzed, and the decrease in MgO content of inclusions after calcium treatment was confirmed.[36] Their later study showed that Mg from the inclusions can go back into the molten steel and can subsequently form fresh spinels by reoxidation.[37] Pretorius *et al.*[38] performed industrial trials and concluded that $MgO\text{-}Al_2O_3$ spinel inclusions can be modified into liquid zones in the $MgO\text{-}Al_2O_3\text{-}CaO$ diagram by calcium treatment. They concluded that the effective modification of spinel inclusions requires low-oxygen potential steel, well-deoxidized slag, and minimum reoxidation at the caster. They also conclude that the modification mechanism is the preferential reduction of the MgO component of spinel to the dissolved Mg into molten steel, and then the residual Al_2O_3 from the spinel inclusions and the resultant CaO react to form liquid inclusions.

It was also reported that the indirect supply of calcium *via* slag could change the morphology and composition of spinel inclusions.[39–43] In these studies, the reaction procedures were as follows: (1) Alumina clusters were formed immediately after the addition of aluminum when the highly basic slag was equilibrated with molten steel killed by aluminum; (2) simultaneously, the reduction of MgO and CaO by the dissolved aluminum occurred to supply soluble Mg and Ca into molten steel; (3) alumina inclusions changed to $MgO{\cdot}Al_2O_3$ inclusions by reacting with the dissolved magnesium; and (4) $MgO{\cdot}Al_2O_3$ inclusions were gradually changed into complex $CaO\text{-}Al_2O_3\text{-}MgO$ inclusions surrounded by softer $CaO\text{-}Al_2O_3$ outer surface layers.

Several papers[22,34–43] all concluded that calcium treatment can successfully modify irregular-shape spinel inclusions into globular $CaO\text{-}Al_2O_3\text{-}MgO$ inclusions, and the authors[36–38,40–42] suggested a similar modification mechanism: (1) replacement of the MgO component of spinel into dissolved Mg by the dissolved Ca; (2) diffusion of the dissolved Mg into molten steel; and (3) the residual Al_2O_3 in the inclusions react with CaO to form liquid inclusions. According to this modification mechanism, when the original irregular and sharp spinel inclusions are reduced by the dissolved Ca, reactions should occur at the sharp edges and then the $Al_2O_3\text{-}MgO$ spinel core will change into a rough spherical shape, as the route 1 and route 2 illustrated in Figure 1. Furthermore, the resulting inclusion by this modification mechanism should be $CaO\text{-}Al_2O_3\text{-}MgO$ or $CaO\text{-}Al_2O_3$, and it should be uniform in composition.

However, most of these authors also showed that the resulting $CaO\text{-}Al_2O_3\text{-}MgO$ inclusions were inhomogeneous in composition, containing 2 to 3 phases—the liquid $CaO\text{-}Al_2O_3$ outer layer and the irregular- and sharp-shaped $Al_2O_3\text{-}MgO$ spinel core, which is opposite to the mechanism suggested by the studies.[22,34–43] These photos were shown in Figure 2 and in the schematic in route 3 in Figure 1. Furthermore, the resulting inclusions with $Al_2O_3\text{-}MgO$ spinel core are still detrimental to the property of the steel. So, modification mechanisms other than those suggested should be developed.

In the current article, a thermodynamic calculation was performed to study the formation of $MgO{\cdot}Al_2O_3$

Table II. Reported Formation Mechanisms of $MgO{\cdot}Al_2O_3$ Inclusions in Steel

Authors		Main Work	Mechanism	Reference(s)
1	Itoh *et al.*	– The deoxidation equilibrium with Mg in liquid iron and the evaluation of the activities of dissolved oxygen and magnesium. – Stability phase diagrams of MgO-$MgO{\cdot}Al_2O_3$ as a function of dissolved magnesium, aluminum, and oxygen in liquid iron and temperature. – Considering the first and the second-order interaction parameters.	Direct reaction	[22,23]
2	Fujii *et al.*	– The free energies for the formation of MgO and $MgO{\cdot}Al_2O_3$. – The phase stability diagram of spinel formation in liquid steel, assuming the activity of $MgO{\cdot}Al_2O_3$ was 0.8 and 0.47.	Direct reaction	[24]
3	Seo *et al.*	– The deoxidation equilibrium among Mg, Al, and O in liquid iron in the presence of $MgO{\cdot}Al_2O_3$ spinel at 1873 K (1600 °C). – Experiments of adding Al and Mg alloys into liquid iron in MgO and Al_2O_3 crucibles. – Determination of the equilibrium constant K_{Mg} and the first- and second-order interaction parameters between Mg and O. – Stability diagram for MgO, $MgO{\cdot}Al_2O_3$, and Al_2O_3 phases at 1873 K (1600 °C) as a function of dissolved Mg, Al, and O contents.	Direct reaction	[25]
4	Todoroki and colleagues	– Alumina clusters formed after the addition of Al into the molten steel; simultaneously, the reduction of MgO in the slag occurred to raise Mg content in the steel, resulting in the change in inclusion composition to $MgO{\cdot}Al_2O_3$ spinel. – The MgO in the slag is chemically reduced by the Al in the molten steel, and the deoxidation product Al_2O_3 reacts with the Mg in the steel that was formed by the chemical reduction of the slag.	Al-reduction reaction	[26–29]
5	Okuyama *et al.*	– MgO concentration in inclusions increases after Al addition until the MgO concentration of the inclusions reaches 25 to 27 mass pct, and Al_2O_3 concentration in the inclusions decreases. – Kinetic model on formation of $MgO{\cdot}Al_2O_3$ inclusion.	Al-reduction reaction	[30]
6	Brabie	– The reduction of MgO by C in the refractory and generate gas phase of magnesium metal $Mg_{(g)}$. – $Mg_{(g)}$ diffuses into metal and reacts with $Al_2O_{3(s)}$ to form $MgO{\cdot}Al_2O_3$ spinel inclusions.	C-reduction	[18,31]
7	Park	– With MgO and Al_2O_3 increasing, the spinel phase is crystallized in the silicate matrix at this stage, and finally the spinel crystals grow during the cooling of the steel melt.	Si-reduction model	[19,20]

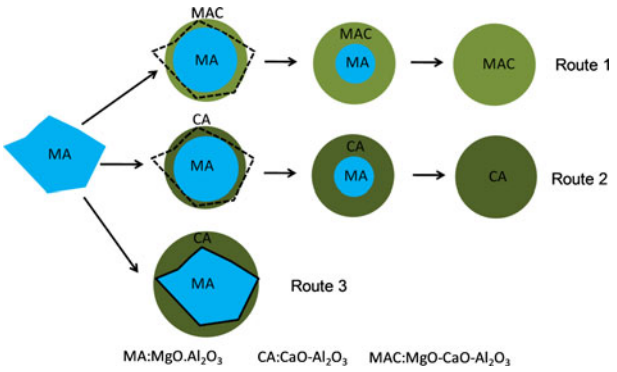

Fig. 1—Possible mechanisms for the modification of $MgO{\cdot}Al_2O_3$ inclusions by Ca treatment.

spinel inclusions in alloy steels. Then, both laboratory experiments and industial trials were carried out to study the modification of $MgO{\cdot}Al_2O_3$ spinels by Ca treatment, and the possible modification mechansim was discussed.

II. THERMODYNAMIC FUNDAMENTALS

To obtain the stability diagrams of Mg-Al-O system, the thermodynamic calculations for the formation of MgO inclusion, Al_2O_3 inclusion, and $MgO{\cdot}Al_2O_3$ inclusion in the molten steel were performed.

For the formation of MgO inclusion,the reaction is[12]

$$(MgO) = [Mg] + [O] \quad [1]$$

$$\log K_1 = -4.28 - 4700/T \quad [2]$$

The equilibrium constant can be expressed by Eq. [3] if both the first-order and the second-order activity interaction coefficients are included.

$$\begin{aligned}\log K &= \log f_{Mg} + \log[\text{pct Mg}] + \log f_O \\ &\quad + \log[\text{pct O}] - \log a_{MgO} \\ &= \left(e_{Mg}^{Mg} + e_O^{Mg}\right)[\text{pct Mg}] + \left(e_{Mg}^{Al} + e_O^{Al}\right)[\text{pct Al}] \\ &\quad + \left(e_{Mg}^{O} + e_O^{O}\right)[\text{pct O}] \\ &\quad + \log[\text{pct Mg}] + \log[\text{pct O}] \\ &\quad - \log a_{MgO} + r_{Mg}^{O}[\text{pct O}]^2 \\ &\quad + \left(r_{Mg}^{MgO} + r_O^{MgO}\right)[\text{pct Mg}][\text{pct O}] \\ &\quad + r_O^{Mg}[\text{pct Mg}]^2 + r_O^{Al}[\text{pct Al}]^2 \\ &\quad + \left(r_O^{Al_2O_3} + r_{Mg}^{Al_2O_3}\right)[\text{pct Al}][\text{pct O}] \\ &\quad + r_O^{(Mg,Al)}[\text{pct Mg}][\text{pct Al}] \end{aligned} \quad [3]$$

For the formation of Al_2O_3 inclusion, the reaction is[12]

$$(Al_2O_3) = 2[Al] + 3[O] \quad [4]$$

$$\lg K_4 = 11.62 - 45,300/T \quad [5]$$

The equilibrium constant can be expressed by Eq. [6]

$$\begin{aligned}\log K &= 2\log f_{Al} + 2\log[\text{pct Al}] + 3\log f_O \\ &\quad + 3\log[\text{pct O}] - \log a_{Al_2O_3} \\ &= \left(2e_{Al}^{Mg} + 3e_O^{Mg}\right)[\text{pct Mg}] + \left(2e_{Al}^{Al} + 3e_O^{Al}\right)[\text{pct Al}] \\ &\quad + \left(2e_{Al}^{O} + 3e_O^{O}\right)[\text{pct O}] + 2\log[\text{pct Al}] \\ &\quad + 3\log[\text{pct O}] - \log a_{Al_2O_3} + 2r_{Al}^{O}[\text{pct O}]^2 \\ &\quad + \left(2r_{Al}^{Al_2O_3} + 3r_O^{Al_2O_3}\right)[\text{pct Al}][\text{pct O}] \\ &\quad + 3r_O^{Al}[\text{pct Al}]^2 + 3r_O^{Mg}[\text{pct Mg}]^2 \\ &\quad + \left(3r_O^{MgO} + 2r_{Al}^{MgO}\right)[\text{pct Mg}][\text{pct O}] \\ &\quad + 3r_O^{(Mg,Al)}[\text{pct Mg}][\text{pct Al}] \end{aligned} \quad [6]$$

For the formation of Al_2O_3 inclusion, the reaction is[12]

$$(MgO \cdot Al_2O_3) = 2[Al] + [Mg] + 4[O] \quad [7]$$

$$\log K_7 = 6.736 - 51083.2/T \quad [8]$$

$$\begin{aligned}\log K &= \log f_{Mg} + 2\log f_{Al} + 4\log f_O + \log[\text{pct Mg}] \\ &\quad + 2\log[\text{pct Al}] + 4\log[\text{pct O}] - \log a_{MgO\times Al_2O_3} \\ &= \left(e_{Mg}^{Mg} + 2e_{Al}^{Mg} + 4e_O^{Mg}\right)[\text{pct Mg}] \\ &\quad + \left(e_{Mg}^{Al} + 2e_{Al}^{Al} + 4e_O^{Al}\right)[\text{pct Al}] \\ &\quad + \left(e_{Mg}^{O} + 2e_{Al}^{O} + 3e_O^{O}\right)[\text{pct O}] + \log[\text{pct Mg}] \\ &\quad + 2\log[\text{pct Al}] + 4\log[\text{pct O}] - \log a_{MgO\times Al_2O_3} \end{aligned} \quad [9]$$

The first and the second interaction confficients were reported by different studies.[6–9] The stability diagrams of Al-Mg-O system were then calculated using these data and are shown in Figure 3. The current calculation (Figure 3(a)) agrees well with that by Itoh *et al.*[6] (Figure 3(b)). Figure 3(c) shows that a lower temperature makes the regions of $MgO{\cdot}Al_2O_3$ and Al_2O_3 larger but makes the region MgO smaller within the same range of dissolved Mg and Al in the molten steel. As shown in Figure 3(d), if the activity of oxide is smaller than 1, then the $MgO{\cdot}Al_2O_3$ region becomes narrower and the MgO region is wider. The formation of $MgO{\cdot}Al_2O_3$ spinel inclusions is also affected by the dissolved oxygen in the steel.

These stability diagrams can be used to predict the correct steel composition for the formation of different oxides. For 30CrMo steel (with composition shown in Table III) with 0.035 pct dissolved Al, when the dissolved Mg in the steel ranges from 0.8 ppm to 10 ppm, $MgO{\cdot}Al_2O_3$ inclusions are formed, and Al_2O_3 inclusions are formed only when the dissolved Mg in the steel is less 0.8 ppm.

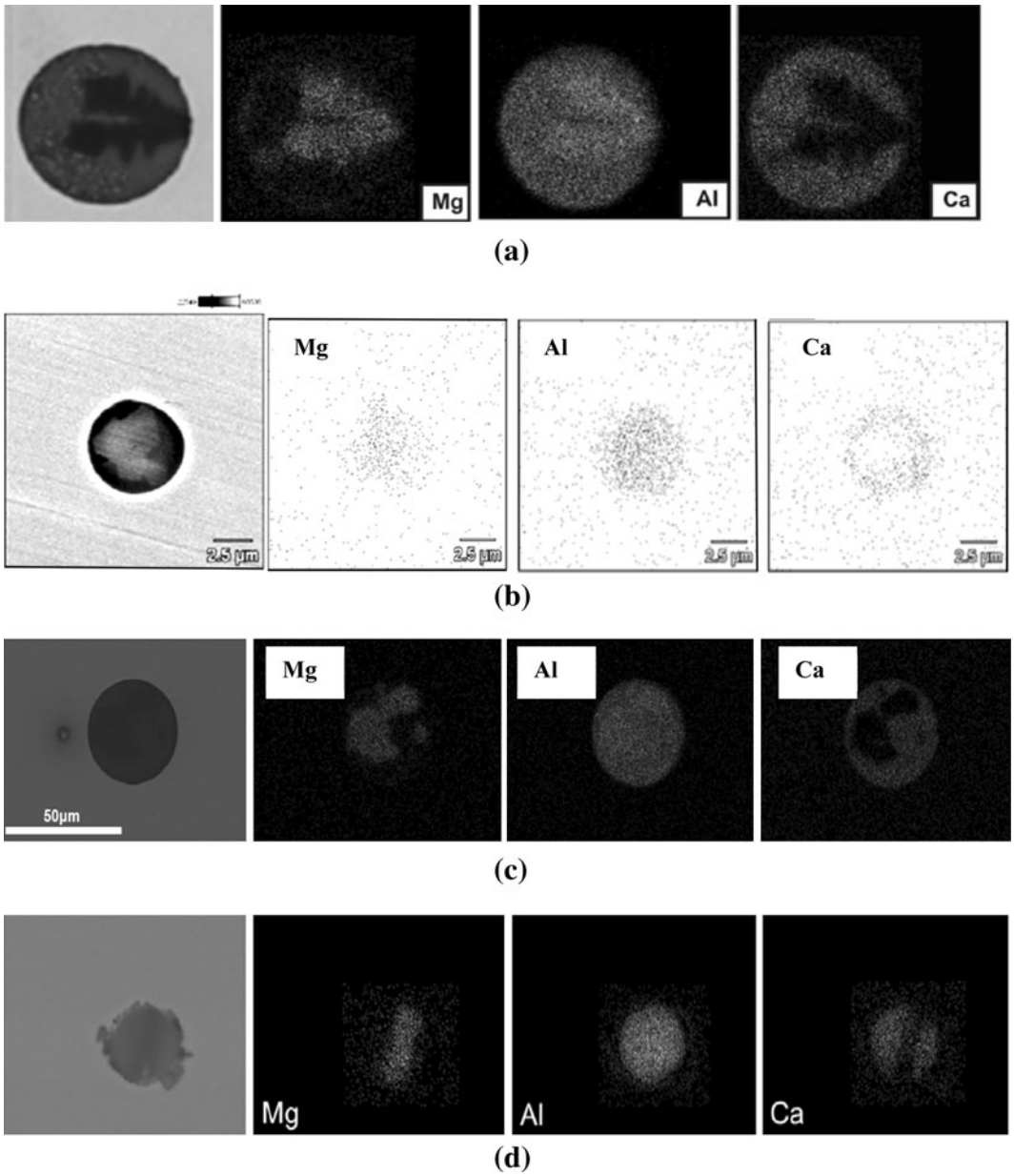

Fig. 2—Morphology and composition of $MgO\text{-}Al_2O_3\text{-}CaO$ inclusions reported by other researchers: (*a*) Michelic *et al.*,[43] 10 min calcium treatment, a spherical inclusion with an irregular shape $MgO{\cdot}Al_2O_3$ core, and an outer $CaO\text{-}Al_2O_3$ layer. (*b*) Jiang *et al.*,[41] 30 min calcium treatment, a spherical inclusion with an irregular shape $MgO{\cdot}Al_2O_3$ core, and an outer $CaO\text{-}Al_2O_3$ layer. (*c*) YoungJo *et al.*,[34] 60 min calcium treatment, a spherical inclusion with an irregular shape $MgO{\cdot}Al_2O_3$ core, and an outer $CaO\text{-}Al_2O_3$ layer. (*d*) Verma *et al.*,[36] with calcium treatment, a spherical inclusion with an irregular shape $MgO{\cdot}Al_2O_3$ core, and an outer $CaO\text{-}Al_2O_3$ layer. (*e*) Martín *et al.*,[45] a spherical inclusion with an irregular shape $MgO{\cdot}Al_2O_3$ core and an outer $CaO\text{-}Al_2O_3$ layer. (*f*) Jiang *et al.*,[46] 180 min calcium treatment, a spherical inclusion with an irregular shape $MgO{\cdot}Al_2O_3$ core, and an outer $CaO\text{-}Al_2O_3$ layer. (*g*) Park,[47] no calcium treatment, with triangle precipitates of $MgO{\cdot}Al_2O_3$ within the $CaO\text{-}SiO_2\text{-}MgO{\cdot}Al_2O_3$ matrix. (*h*) Björklund *et al.*,[48] no calcium treatment, with triangle precipitates of $MgO{\cdot}Al_2O_3$ within the inclusion matrix.

III. LABORATORY EXPERIMENTS OF MODIFICATION OF $MgO{\cdot}Al_2O_3$ INCLUSIONS USING CALCIUM TREATMENT

A 6-kg vacuum induction furnace was used to remelt 30CrMo steel samples and a vertical Si-Mo heated resistance furnace was used for calcium treatment. The experimental procedures were as follows:

- Melt 280 g steel (with composition shown in Table III) in a MgO crucible at 1873 K (1600 °C) under argon atmosphere.
- Add 0.3 g aluminum wires into the molten steel for deoxidation.
- After 5 minutes, add 2.6 g MgSi powders to the molten steel to generate $MgO{\cdot}Al_2O_3$ inclusions.
- After 10 minutes, add a certain amount of CaSi powders to modify $MgO{\cdot}Al_2O_3$ inclusions (case 1: no Si-Ca added; case 2: 0.6 g SiCa added; and case 3, 1.0 g SiCa added).
- After 60 minutes, take a steel sample using quartz tubes and quench it in water quickly, so the time of calcium treatment in the laboratory is 60 minutes.

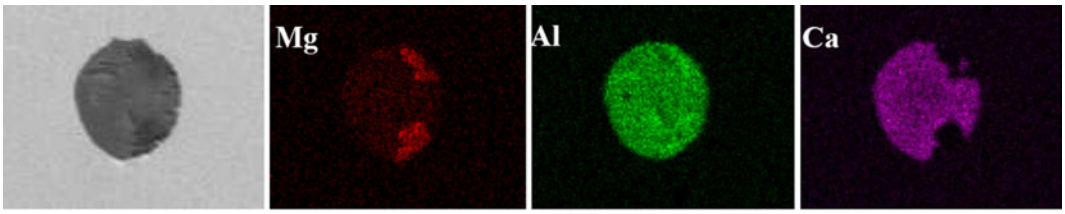

(e)

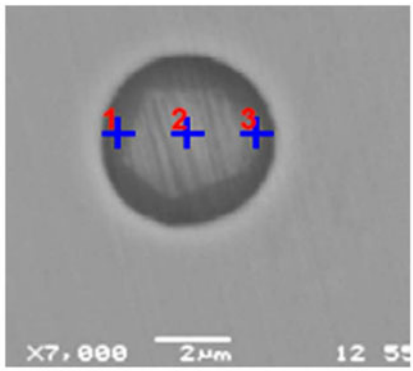

Point 1: MgO: 12.5%, Al_2O_3:48.1%, CaO: 39.4%

Point 2: MgO: 29.4%, Al_2O_3:68.4%, CaO: 2.2%

Point 3: MgO: 18.5%, Al_2O_3:54.4%, CaO: 27.1%

(f)

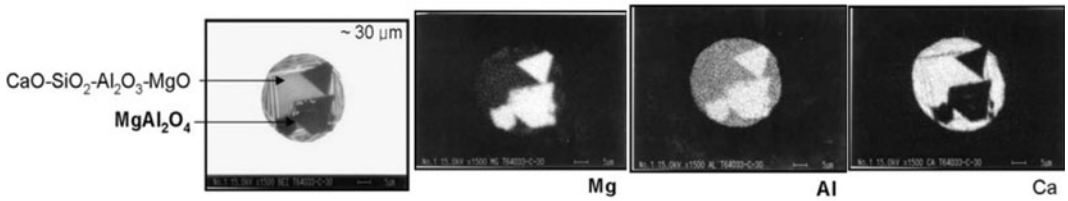

(g)

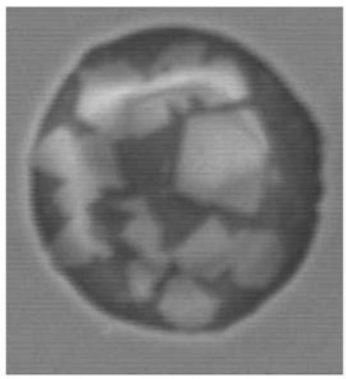

(h)

Fig. 2—continued.

Each experiment was repeated once, and at each step, steel samples were taken using quartz tubes. The chemical compositions in the steel samples were analyzed by inductively coupled plasma-atomic emission spectroscopy, and the inclusions were analyzed by scanning electron microscopy (SEM)-energy-dispersive X-ray spectroscopy (EDX) and an optical microscope. For one sample, the compositions and morphology of 40 inclusions were analyzed by SEM-EDX and sizes of 1000 inclusions were observed by optical microscope manually. The compositions of the steel before and after the experiments were shown in Table IV. With more CaSi added, there were more dissolved magnesium and less total oxygen in the steel, indicating that the MgO in the spinel inclusions was, at least partially, reduced into dissolved magnesium. The increasing aluminum in the steel may come from the dissolution of the Al_2O_3 component of the inclusions.

Figure 4 shows the composition of inclusions, by EDX area scanning, in the steel with and without calcium treatment; in Figure 4, the region of the red circle is the liquid region. As shown in Figure 4(a), most of

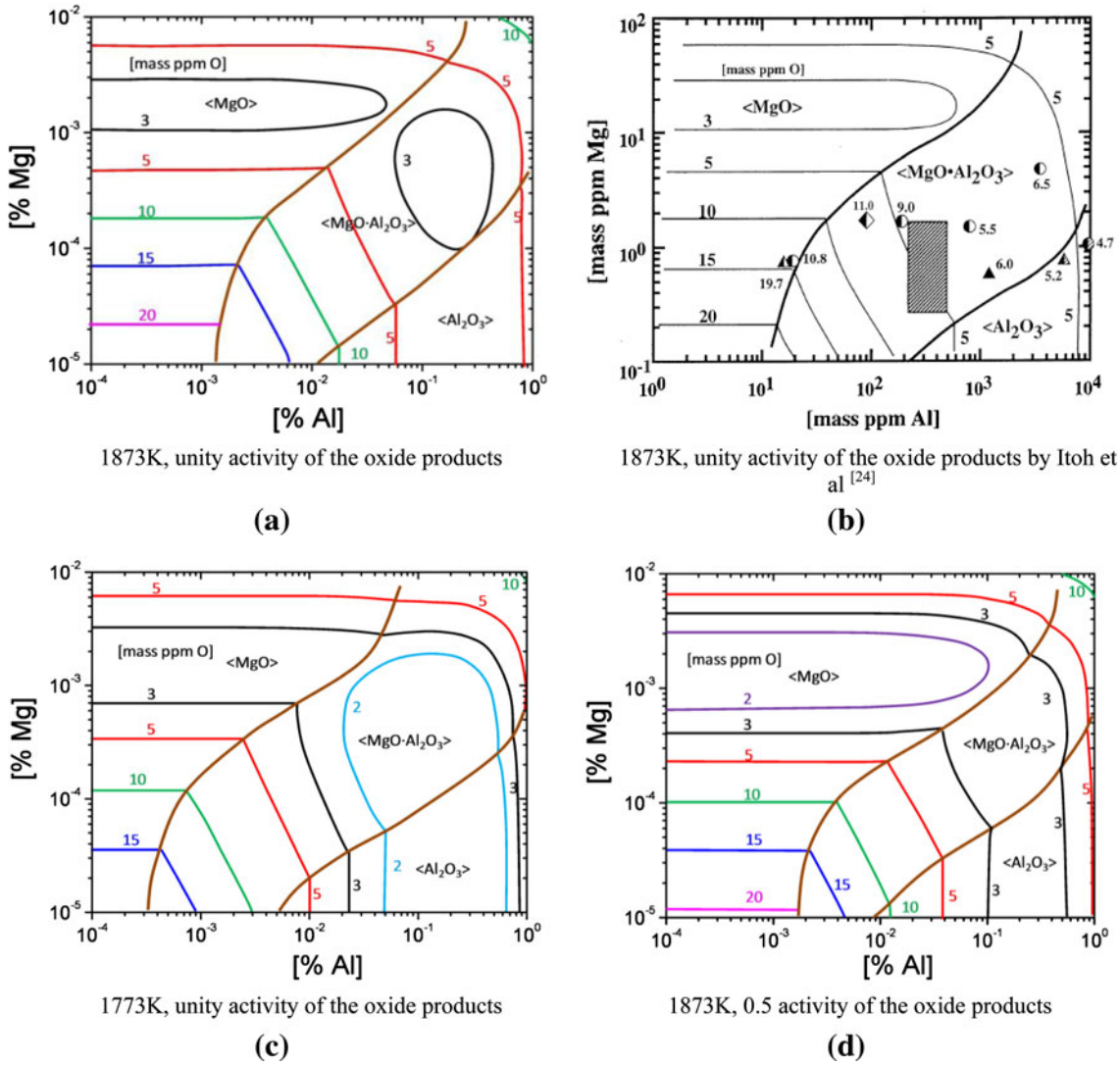

Fig. 3—Calculated stability diagram of Mg-Al-O system in the molten steel.

Table III. Composition of 30CrMo Steel (pct)

C	Si	P	S	Mn	Al	Cr	Mo
0.34	0.35	0.20	0.015	0.70	0.035	0.10	0.20

Table IV. The Composition of the Steel in the Laboratory Experiments (Weight Percent)

	First Experiment				Second Experiment			
	Ca	Mg	Al	T.O.	Ca	Mg	Al	T.O.
Case 1	<0.0005	0.0007	0.030	0.0024	<0.0005	0.0009	0.027	0.0025
Case 2	0.0007	0.0008	0.035	0.0023	0.0005	0.0009	0.030	0.0025
Case 3	0.0012	0.0010	0.036	0.0023	0.0020	0.0013	0.033	0.0023

Note: Case 1: no Si-Ca was added; case 2: 0.6 g SiCa was added; and case 3: 1.0 g SiCa was added to 280 g steel.

the inclusions before Ca treatment were $MgO{\cdot}Al_2O_3$, and the content of MgO in the inclusions varied within 5 pct to 28 pct. Figure 4(b) shows that when adding 0.6 g SiCa powders to the 280 g steel, approximately 50 pct of inclusions were in the liquid region of the $MgO\text{-}Al_2O_3\text{-}CaO$ system. Figure 4(c) indicates that when adding 1 g SiCa powders into the 280 g steel, most of the resulting $MgO\text{-}Al_2O_3\text{-}CaO$ inclusions were liquid.

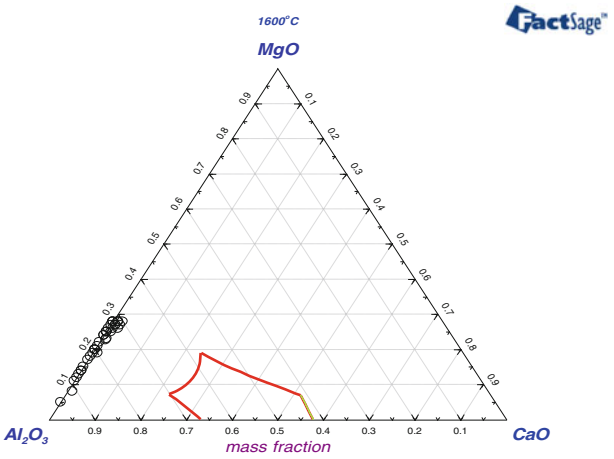

Case 1:No SiCa powder added

(a)

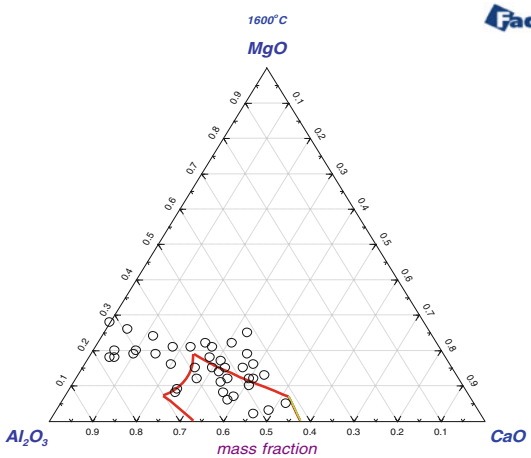

Case 2: 0.6 g SiCa powder added

(b)

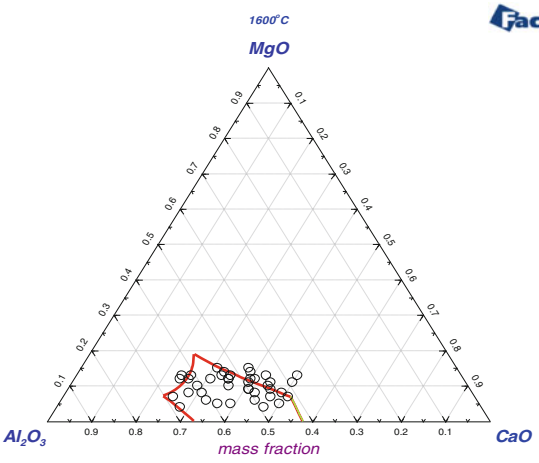

Case 3: 1 g SiCa powder added

(c)

Fig. 4—Composition of inclusions in steel samples.

Figure 5 shows that inclusions without calcium treatment were mainly irregular in shape, either triangle, rectangular, or square shape, and after calcium treatment, most of the inclusions were spherical because the liquid feature has the effect of surface tension to hold the droplets in spherical shape. Thus, from the changes of inclusion composition and morphology before and after Ca treatment, it can be inferred that $MgO{\cdot}Al_2O_3$ inclusions were probably modified into liquid the MgO-Al_2O_3-CaO inclusions. Figure 6 shows that before calcium treatment, most of the inclusions were smaller than 3 μm, and after the calcium treatment, inclusions were mainly 2 to 5 μm. Inclusions in the steel with calcium treatment were a little larger than that without calcium treatment. Approximately 70 pct of inclusions are less than 2 μm before Ca treatment; however, only about 20 pct inclusions are less 2 μm after Ca treatment. It should be noticed that if only the MgO in the $MgO{\cdot}Al_2O_3$ inclusions was reduced during Ca treatment, the size of inclusions should change little. Because the size of inclusions became bigger after calcium treatment, there should be other reactions other than the reducing of MgO by the dissolved calcium occurred during Ca treatment.

Figure 7(a) shows the elemental mapping of a 5-μm $MgO{\cdot}Al_2O_3$ inclusion before Ca treatment. Before Ca treatment, the distribution of MgO and Al_2O_3 was uniform across the entire cross section of the inclusions. This figure also indicates that the pure $MgO{\cdot}Al_2O_3$ inclusion was nonspherical.

Figure 7(b) shows the elemental mapping of a ~8-μm CaO-MgO-$\cdot Al_2O_3$ inclusion after Ca treatment, indicating that (1) there was no MgO at the location where CaO existed; (2) CaO always stayed at the outside layer of the inclusion, and the outer CaO-containing layer was averagely a quarter of the diameter of the inclusion; (3) MgO existed in the core of the inclusion, and the concentration of MgO decreased outward along the radius from the center, which implies the noncomplete reducing of MgO by the dissolved calcium, $(MgO) + [Ca] \rightarrow [Mg] + (CaO)$, in the steel; and (4) Al_2O_3 distributed everywhere of the inclusion but more Al_2O_3 stayed with MgO in the core, less stayed in the outside layer with CaO, and the region of Al_2O_3 was larger than that of MgO core, which implies again the noncomplete reducing of MgO by the dissolved calcium in the steel. The formation of the inclusion in Figure 7(b) is similar to that of Figure 1 (route 2) and that of Figure 2(b).

Figure 7(c) shows another typical ~10-μm CaO-MgO-$\cdot Al_2O_3$ inclusion after calcium treatment, which has the following features:

(a) MgO component was not in the center of the inclusion and was in irregular shape.
(b) There was no MgO at the location where CaO existed.
(c) Al_2O_3 was uniformly distributed everywhere in the inclusion.

This kind of resulting inclusion is hardly explained by the reducing reaction $(MgO) + [Ca] \rightarrow [Mg] + (CaO)$ because the MgO core is not in the center and not spherical. This inclusion is more like that of Figure 1 (route 3) and Figures 2(a) and (c) through (e). Other formation mechanisms, other than the reducing reaction, should be suggested.

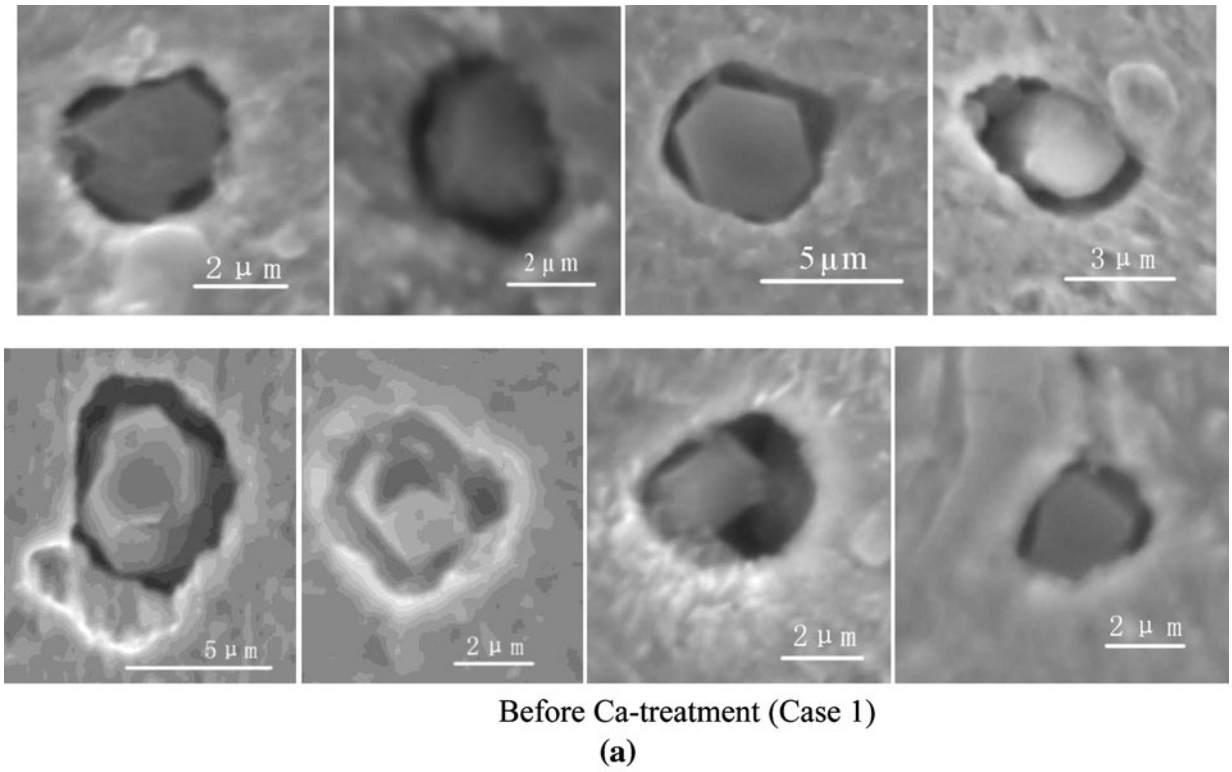

Fig. 5—Morphology of inclusions in steel samples of laboratory experiments: (*a*) before Ca treatment (case 1) and (*b*) After Ca treatment (case 2).

Most of the inclusions after calcium treatment showed the similar distribution of MgO, Al_2O_3, and CaO like those of Figures 7(b) and (c). Inclusions with a uniform distribution of MgO, Al_2O_3, and CaO within their entire cross section are rare, like that illustrated by Figure 1 (route 2). The refining time of the current Ca treatment experiments was 60 minutes. Laboratory experimental results indicate that within this calcium treatment time, $MgO{\cdot}Al_2O_3$ inclusions can be hardly fully modified into liquid MgO-Al_2O_3-CaO inclusions or liquid Al_2O_3-CaO inclusions.

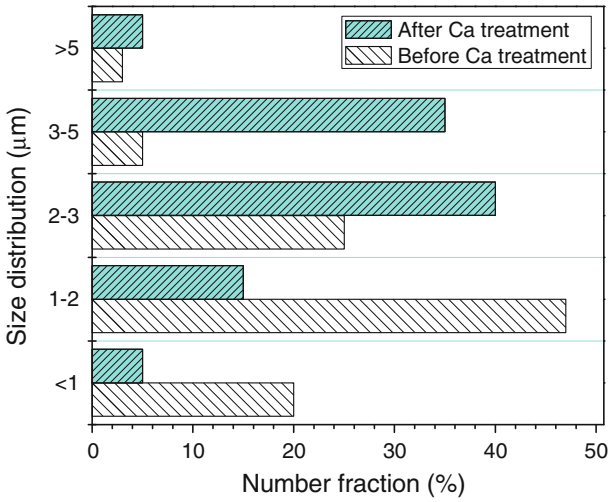

Fig. 6—Size distribution of inclusions before and after Ca treatment of laboratory experiments.

Figure 8 shows $MgO\text{-}Al_2O_3$–CaS inclusions after calcium treatment, indicating that (1) a $MgO\text{-}Al_2O_3$ spinel inclusion with CaS after calcium treatment was not spherical rather, it kept the original irregular shape; (2) MgO and Al_2O_3 stayed in the core of the inclusions, and CaS stayed at the outer layer of the inclusions; and (3) no MgO was found at the location where CaS existed. The composition distribution of this inclusion implies that the reducing reaction (MgO) + [Ca] → [Mg] + (CaO) is not the only formation mechanism.

IV. INDUSTRIAL TRIALS OF THE MODIFICATION OF $MgO{\cdot}Al_2O_3$ INCLUSIONS USING CALCIUM TREATMENT

In the industrial trial, the composition of the 30CrMo steel was (in weight percent) as follows: C 0.30, Si 0.22, Mn 0.52, P 0.015, S 0.007, Mo 0.10, V 0.12, Cu 0.07, Cr 0.94, and the dissolved aluminum Al_s 0.020. The production route was 100t electric arc furnace→ladle furnace refining (LF) with CaSi treatment→vacuum degassing (VD) →210 mm billet continuous casting. The refining time was ~60 minutes at LF and 40 minutes at VD. During tapping, 300 kg Al, 800 kg SiMn, and 400 kg FeMn were added to the steel melt for deoxidation. A 200-m CaSi wire with a 0.8 cm diameter and containing 34.5 pct calcium was added into the molten steel 2 minutes after the start of the LF refining. After 30 minutes of LF treatment, 60 kg Al wire, 56 kg FeMn, 113 kg FeMo, and 180 kg FeCr alloys were added to adjust the composition of the molten steel. Four heats were performed during the industrial trials. The samples were taken before calcium treatment, 30 minutes after calcium treatment, and 60 minutes after calcium treatment. During sampling, the samplers were immersed 300 mm beneath the surface of the molten steel. Inclusions in the steel samples were observed and analyzed using SEM-EDS. Figures 9 and 10 shows the morphology of inclusions in the steel before and after calcium treatment by LF refining process. It is clearly indicated that many inclusions in the steel before calcium treatment were nonspherical, whereas after calcium treatment, most of the inclusions were modified into spherical shapes. The composition of inclusions, by EDX area scanning, in the steel during LF refining is detected, and the $CaO\text{-}MgO\text{-}Al_2O_3$ ternary composition is shown in Figure 11. The inclusions detected were mainly pure Al_2O_3 inclusions, $MgO{\cdot}Al_2O_3$ spinels, $CaO\text{-}Al_2O_3$ inclusions, and $MgO\text{-}Al_2O_3\text{-}CaO$ complex inclusions. Before LF treatment, there were many pure Al_2O_3 inclusions and $MgO{\cdot}Al_2O_3$ spinel inclusions. After 30 minutes of refining, pure $MgO{\cdot}Al_2O_3$ spinel inclusions disappeared, the content of CaO in the inclusions increased, and the content of MgO in the inclusions decreased. Because of the calcium treatment, more liquid inclusions, in the region of the red circle in Figure 11, appeared. After 30 minutes of calcium treatment, the average composition of inclusions was 51.48 pct Al_2O_3, 3.69 pct MgO and 44.51 pct of CaO. After 60 min calcium treatment, the content of CaO in the inclusions was decreased, which was because at 30 min several kinds of alloys including aluminum alloys were added into the steel, and 10 minutes more refining were performed. The MgO content in the inclusions were decreased with time during LF refining.

In the industrial trials, the inhomogeneous composition distribution on the $MgO\text{-}Al_2O_3\text{-}CaO$ complex inclusions after Ca treatment also was observed. Figure 12 shows the elemental mapping of two $CaO\text{-}MgO{\cdot}Al_2O_3$ inclusions after 40 minutes of Ca treatment in the industrial trials. The composition distribution within these two inclusions is more like that shown in Figure 7(c), with the following features: (1) CaO always stayed at the outside layer of the inclusion, and there was no MgO at the location where CaO existed; (2) MgO existed in the core of the inclusion and the MgO distribution was not spherical but irregular with sharp edges; (3) Al_2O_3 either distributed in the outer layer less than that in the $MgO\text{-}Al_2O_3$ (Figure 12(a)) or distributed uniformly across the entire section of the inclusion (Figure 12(b)). Elemental line scans in Figure 13 also show that MgO and CaO hardly coexisted. The industrial trial also shows that the inclusions after calcium treatment were larger than those before calcium treatment, and the inclusions found in the steel samples of in the industrial trials were larger than those in the steel samples of laboratory experiments.

V. KINETIC ANALYSIS ON MODIFICATION OF $MgO{\cdot}Al_2O_3$ BY CALCIUM TREATMENT

In both the laboratory experiments and industrial trials, the inhomogeneous composition distribution in the $CaO\text{-}MgO\text{-}Al_2O_3$ complex inclusions after Ca treatment was observed. Figures 7, 8, 12, and 13 show that CaO always stayed at the outside layer of the inclusion, MgO existed in the core of the inclusion, and MgO and CaO hardly coexisted. The observation is similar to those by other researchers shown in Figure 2, which shows that even after 60 to 180 minutes of calcium treatment refining, pure $MgO{\cdot}Al_2O_3$ component still

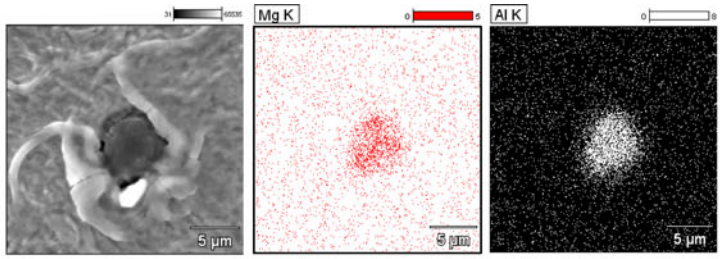

Elemental mapping of $MgO{\cdot}Al_2O_3$ inclusion before Ca-treatment

(a)

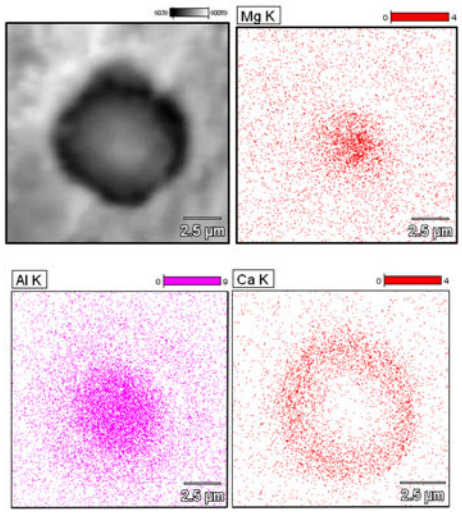

Elemental mapping of an inclusion after Ca-treatment (with a spherical $MgO{\cdot}Al_2O_3$ core and an outer $CaO\text{-}Al_2O_3$ layer, more Al_2O_3 in the core than the outer layer)

(b)

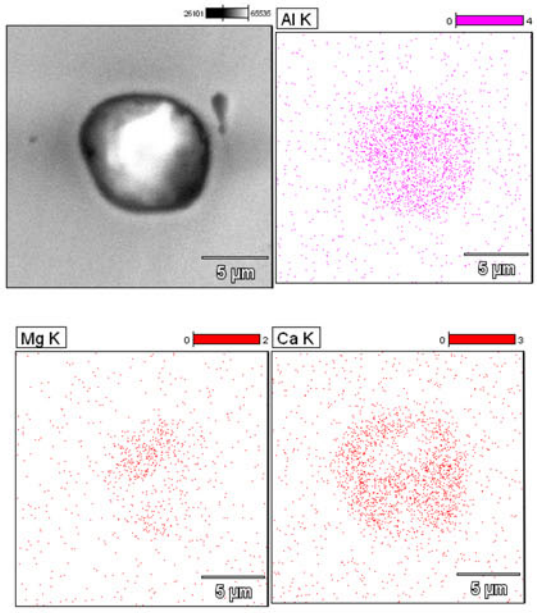

Elemental mapping of an inclusion after Ca-treatment (with an irregular shape $MgO{\cdot}Al_2O_3$ core and an outer $CaO\text{-}Al_2O_3$ layer, uniform Al_2O_3 in the core and the outer layer)

(c)

Fig. 7—Elemental mapping of inclusions before after Ca treatment of laboratory experiments: (*a*) elemental mapping of $MgO{\cdot}Al_2O_3$ inclusion before Ca treatment, (*b*) elemental mapping of an inclusion after Ca treatment (with a spherical $MgO{\cdot}Al_2O_3$ core and an outer $CaO\text{-}Al_2O_3$ layer, more Al_2O_3 in the core than the outer layer), and (*c*) elemental mapping of an inclusion after Ca treatment (with an irregular shape $MgO{\cdot}Al_2O_3$ core and an outer $CaO\text{-}Al_2O_3$ layer, uniform Al_2O_3 in the core and the outer layer).

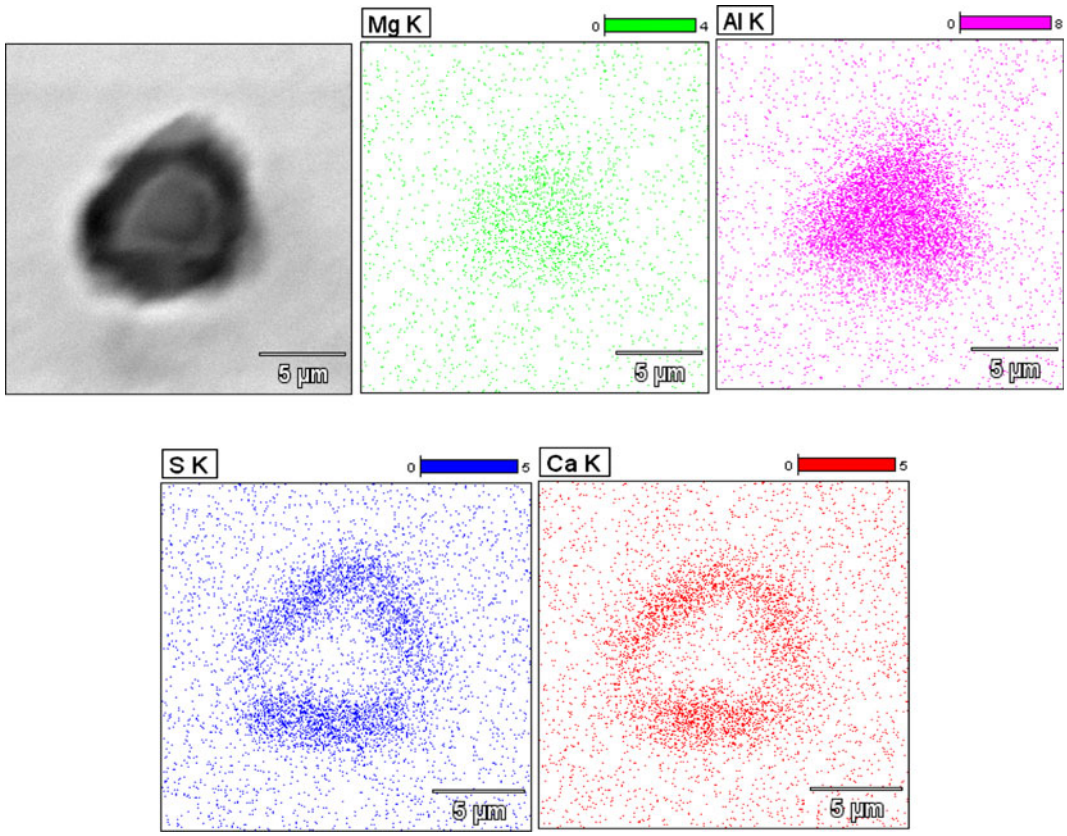

Fig. 8—Elemental mapping of MgO-Al_2O_3–CaS inclusion after Ca treatment of laboratory experiments.

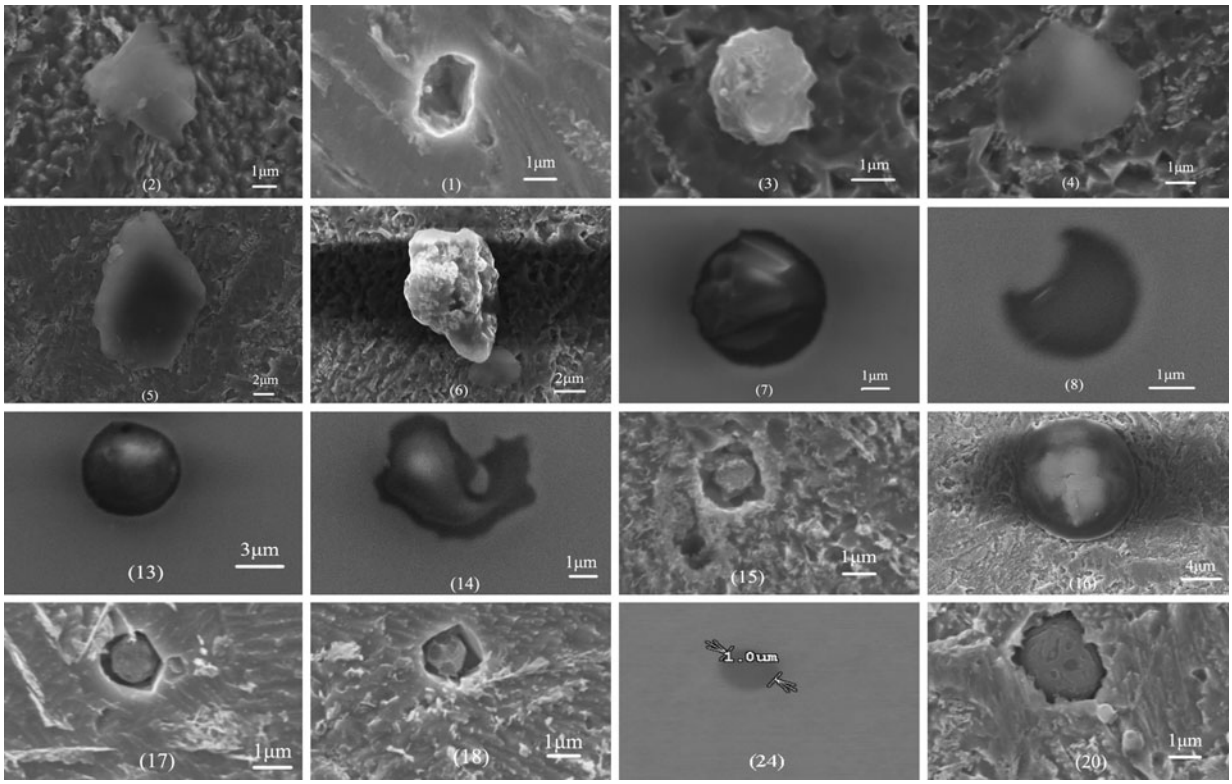

Fig. 9—Morphology of inclusions in the steel before calcium treatment (industrial trial).

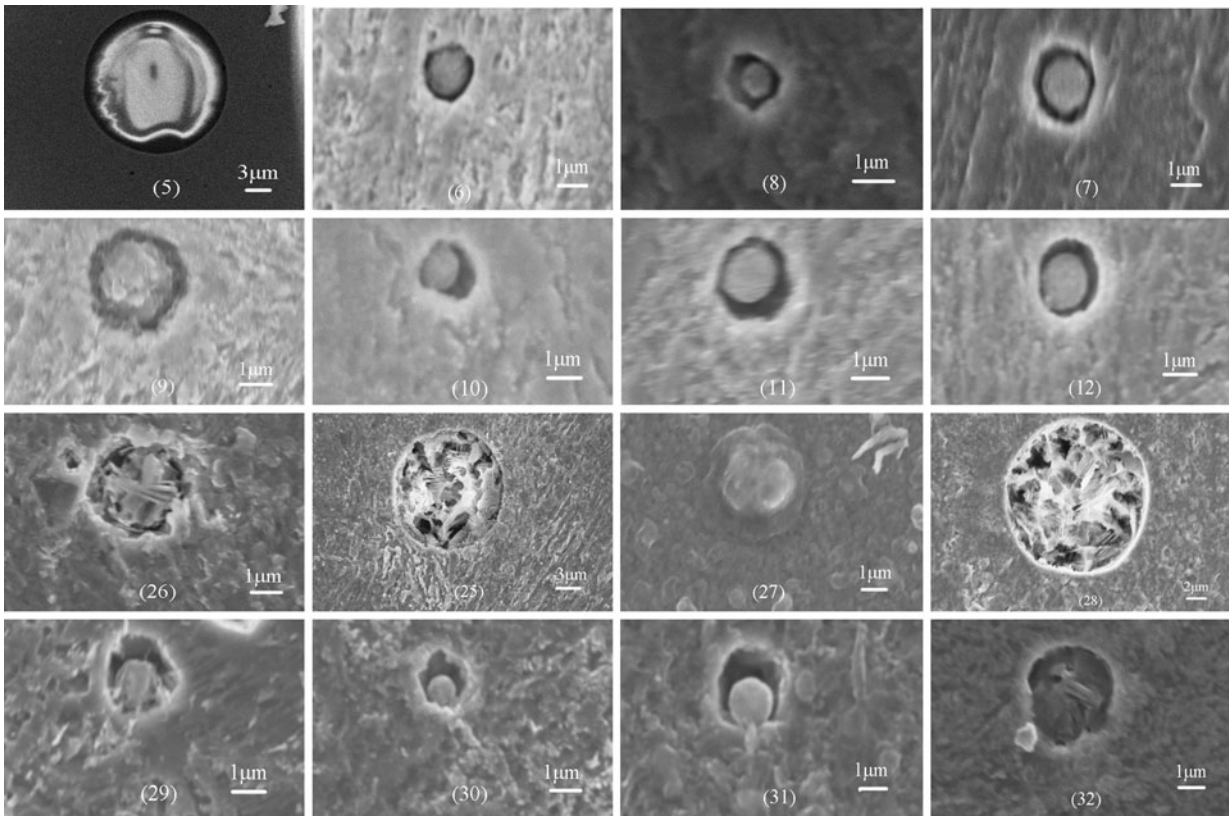

Fig. 10—Morphology of inclusions in the steel after calcium treatment (industrial trial).

existed inside the resulting CaO-MgO-Al_2O_3 inclusion. In addition, it implies that 60 to 180 minutes of calcium treatment could hardly fully modify a MgO·Al_2O_3 inclusion into a uniform CaO-MgO-Al_2O_3 inclusion or CaO-Al_2O_3 inclusion. So, the kinetic condition is one of the key factors to determine whether the reducing reaction (MgO) + [Ca] → [Mg] + (CaO) can proceed or not.

Figure 14 shows the schematic of the kinetic model on the modification of MgO·Al_2O_3 inclusion by Ca treatment with the following steps: (1) diffusion of [Ca] in the molten steel, (2) diffusion of [Ca] in the resulting calcium aluminates, (3) chemical reaction at the liquid steel–inclusion interface, (4) diffusion of [Mg] in calcium aluminates, and (5) diffusion of [Mg] in the molten steel.

It was reported that the diffusion coefficients of Ca in calcium aluminates, Al in the calcium aluminates, and Mg in the spinel are $D_1 = 10^{-8.6}$ m^2/s, $D_2 = 10^{-10.4}$ m^2/s, and $D_3 = 3.2 \times 10^{-13}$ m^2/s, respectively.[44] Thus, the diffusion of Ca in the calcium aluminates is much faster than the diffusion of Al in the calcium aluminates. Because of the similar properties between aluminum and magnesium, the diffusion coefficient of Mg in the calcium aluminates (D_4) should be smaller than the diffusion coefficient of Al in the calcium aluminates ($D_2 = 10^{-10.4}$ m^2/s). The diffusion coefficients of Mg and Ca in the molten steel are approximately $D_4 = 3.5 \times 10^{-9}$.[30] Furthermore, the chemical reaction at the interface is very fast. Thus, the diffusion of Mg in the calcium aluminates is the control step for the modification of MgO·Al_2O_3 by Ca treatment. At the very beginning, the reducing reaction (MgO) + [Ca] → [Mg] + (CaO) occurs, and MgO in the inclusion is partially reduced into the dissolved magnesium. However, as the reaction goes on, a calcium aluminate layer is generated around the inclusion, and the diffusion of Mg within this calcium aluminate layer is slow, which will retard the reducing reaction. Simultaneously, the reaction of (Al_2O_3) + [Ca] + [O] → (xCaO·$y$$Al_2O_3$) occurs all the time, which will generate more and more calcium aluminate layer around the inclusion, and if the xCaO·$y$$Al_2O_3$ phase is liquid, then the inclusion will be in a spherical shape because of the effect of surface tension.

VI. BALANCE OF CALCIUM AND MAGNESIUM IN MOLTEN STEEL AND INCLUSIONS

According to the measured steel composition before and after calcium treatment as listed in Table V, the average total oxygen (T.O.) was 22 ppm before calcium treatment.

Assuming the dissolved oxygen was 1 ppm, the content of oxygen in the inclusion will be 21 ppm before calcium treatment. Then, the amount of oxygen in inclusions in 1 kg steel is $O_a = 21 \times 10^{-6}$ kg. According to an SEM observation in the current study, the average size of MgO·Al_2O_3 inclusions is 5 μm (Figure 9). If it is assumed that all of the inclusions are MgO·Al_2O_3 in the steel, then the amount of oxygen content in one MgO·Al_2O_3 inclusion (O_1) is

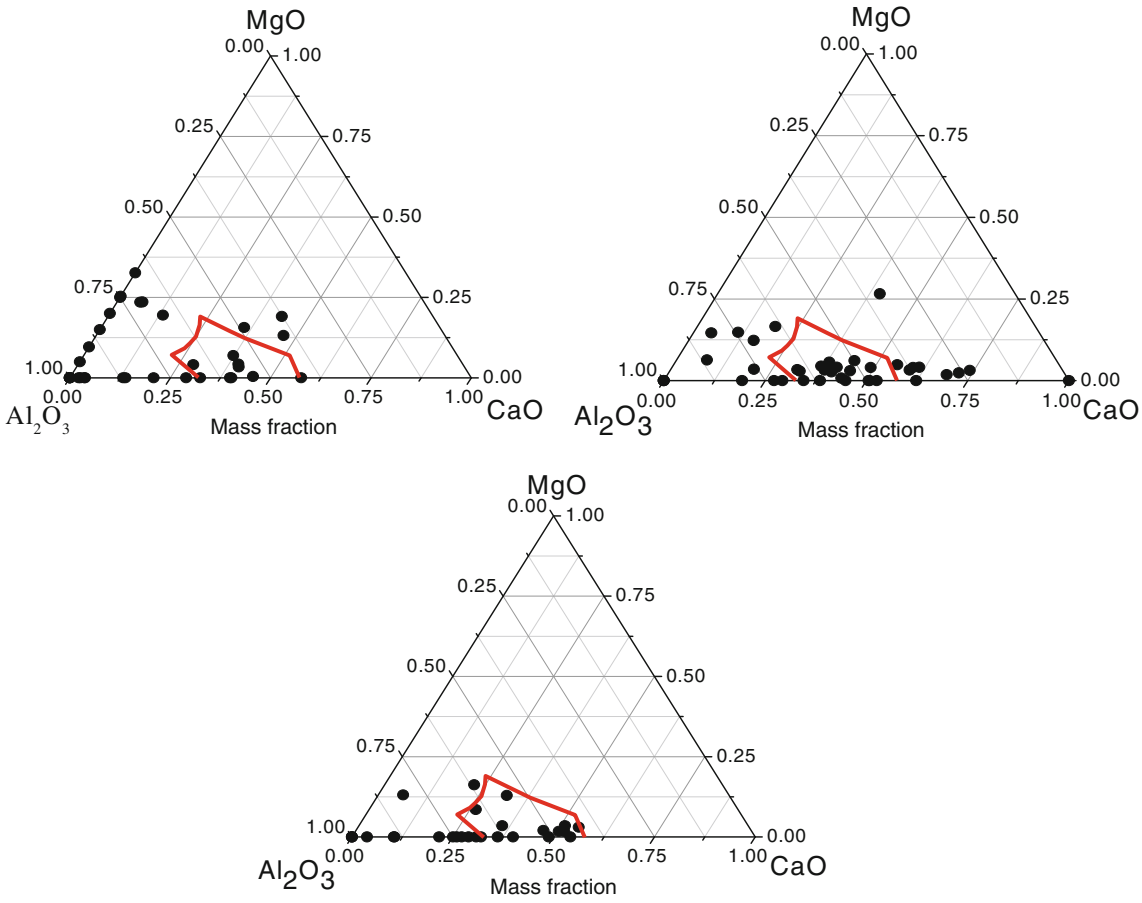

Fig. 11—Composition of inclusions before (left), during (middle), and after (right) calcium treatment in LF refining process.

$$O_1 = \frac{\pi}{6}\left(5 \times 10^{-6}\text{m}\right)^3 \cdot \left(3500\,\text{kg/m}^3\right) \cdot \left(\frac{4M_o}{M_{\text{MgO}\cdot\text{Al}_2\text{O}_3}}\right) = 1.032 \times 10^{-13}\text{kg} \quad [10]$$

where M is the molecular weight of the materials. Then, the number of $MgO{\cdot}Al_2O_3$ inclusions in 1 kg steel n can be expressed by

$$n = \frac{O_a}{O_1} = \frac{21 \times 140^{-6}\ \text{kg}}{1.032 \times 10^{-13}\ \text{kg}} = 2.035 \times 10^8 \quad [11]$$

From the steel composition measured before and after calcium treatment (Table V), the increase of the dissolved magnesium in the steel after calcium treatment is approximately $\Delta[\text{Mg}] = 1.5$ ppm, and the Mg increase in the steel is caused by the reducing reaction (MgO) + [Ca] → [Mg] + (CaO). So, the change of the calcium in one inclusion caused by this reducing reaction is

$$\Delta\text{Ca} = \frac{\Delta[\text{Mg}] \cdot \frac{M_{\text{Ca}}}{M_{\text{Mg}}} \times 10^{-6} \times 1\,\text{kg}}{n} = 1.227 \times 10^{-14}\,\text{kg} \quad [12]$$

Furthermore, according to SEM-EDX detection for the inclusions, the average content of CaO in the inclusions after calcium treatment is 37.5 pct. So, the average fraction of calcium in inclusions is

$$(37.5\,\text{pct}) \cdot \left(\frac{M_{\text{Ca}}}{M_{\text{CaO}}}\right) = 26.78\ \text{pct} \quad [13]$$

The amount of Ca in one inclusion is, $C_{\text{Ca}-1}$

$$C_{\text{Ca}-1} = \frac{\pi}{6}\left(5.0 \times 10^{-6}\ \text{m}\right)^3 \times 3500\,(\text{kg/m}^3) \times 26.78\ \text{pct} = 6.131 \times 10^{-14}\ \text{kg} \quad [14]$$

Comparing Eqs. [12] and [14] indicates that the amount of Ca in inclusions is larger than the amount of Ca produced by the reducing reaction (MgO) + [Ca] → [Mg] + (CaO). Thus, there are other sources of calcium to enter the inclusion during calcium treatment. Quantitatively, 1.227/6.131 = 20 pct of the calcium in the inclusion is from the reducing reaction (MgO) + [Ca] → [Mg] + (CaO), and 80 pct is from the other reactions.

Thus, the modification of $MgO{\cdot}Al_2O_3$ inclusions by calcium treatment includes two steps, as discussed previously:

Step 1: Reducing a part of the MgO of the inclusion into dissolved magnesium by the dissolved calcium in the steel.

Step 2: Generating a liquid $x\text{CaO}{\cdot}y\text{Al}_2\text{O}_3$ layer at the outside of the spinel inclusion.

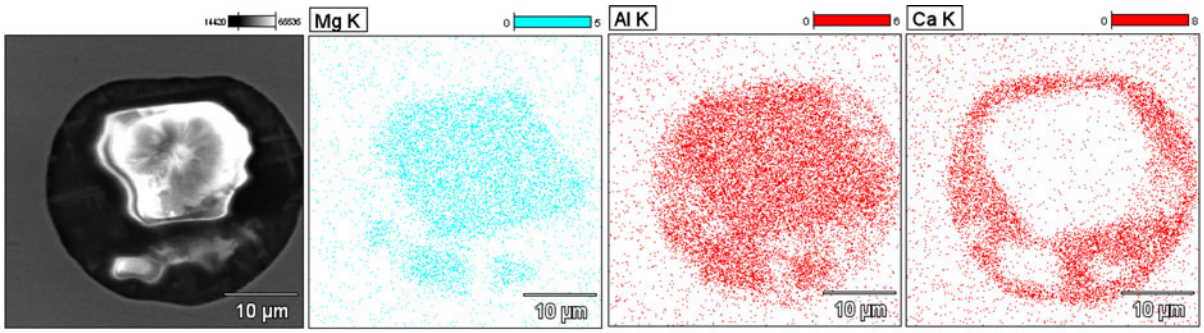

Fig. 12—Elemental mapping of $MgO{\cdot}Al_2O_3$ inclusion after Ca treatment in steel samples of the industrial trial: (*a*) with an irregular shape $MgO{\cdot}Al_2O_3$ core and an outer $CaO\text{-}Al_2O_3$ layer, more Al_2O_3 in the core that in the outer layer and (*b*) with an irregular shape $MgO{\cdot}Al_2O_3$ core and an outer $CaO\text{-}Al_2O_3$ layer, uniform Al_2O_3 in the core and the outer layer.

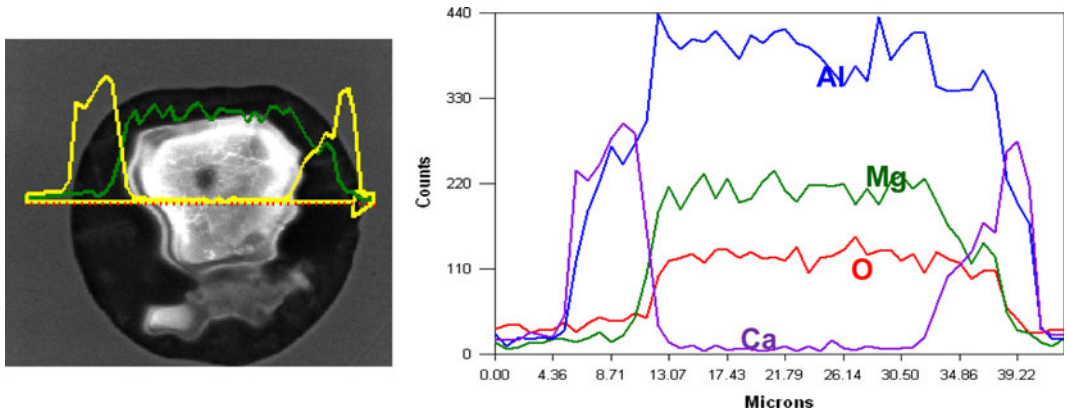

Fig. 13—Elemental line scans of $MgO{\cdot}Al_2O_3$ inclusion after Ca treatment industrial trials.

VII. MECHANISM ON THE MODIFICATION OF $MgO{\cdot}Al_2O_3$ USING CALCIUM TREATMENT

Based on the thermodynamic analysis, the experimental observation, and the preceding discussion, the modification mechanism of the $MgO{\cdot}Al_2O_3$ can be summarized by the following steps and the schematic in Figure 15:

Step 1: Reducing part of MgO in the inclusion into dissolved magnesium by the dissolved calcium in the steel.

The irregular shape $MgO{\cdot}Al_2O_3$ spinel reacts with the dissolved calcium by

$$y(MgO \cdot Al_2O_3) + x[Ca] = (xCaO \cdot yAl_2O_3) + y[Mg] \quad [15]$$

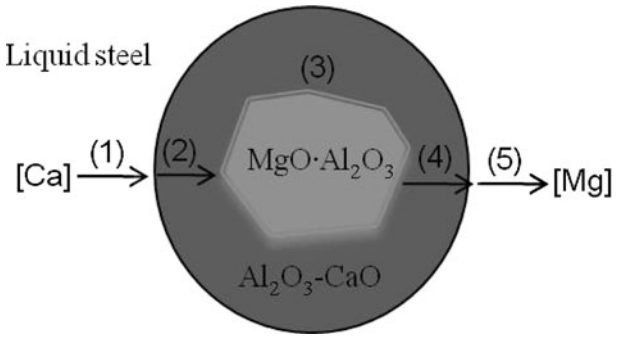

Fig. 14—Schematic of the kinetic model on modification of MgO·Al_2O_3 inclusion by Ca treatment.

Table V. Ca, Mg, Al and the T.O. in Mass pct Before and After Calcium Experiment of the Industrial Trial

	Ca	Mg	Al	T.O.
Before calcium treatment	<0.0005	0.0008	0.0285	0.0022
After calcium treatment	0.0010	0.00095	0.0345	0.0021

By this step, the magnesium in the spinel inclusion is replaced by the dissolved calcium in the steel; and then dissolved magnesium is generated, which enters the molten steel. Gradually, a thin layer of xCaO·$y$$Al_2O_3$ is generated at the outside of the spinel inclusion, and the MgO·Al_2O_3 core of the spinel inclusion becomes a little smaller than its original size. The fact that the magnesium content in the molten steel increased after calcium treatment proves this step.

The following possible reactions are possible during this step:

$$[Ca] + [O] = (CaO) \quad [16]$$

$$[Al] + [O] = (Al_2O_3) \quad [17]$$

$$x[Ca] + 2y[Al] + (x + 3y)[O] = (x\text{CaO} \cdot y\text{Al}_2\text{O}_3) \quad [18]$$

$$x(CaO) + y(Al_2O_3) = (x\text{CaO} \cdot y\text{Al}_2\text{O}_3) \quad [19]$$

$$3(MgO) + 2[Al] = (Al_2O_3) + 3[Mg] \quad [20]$$

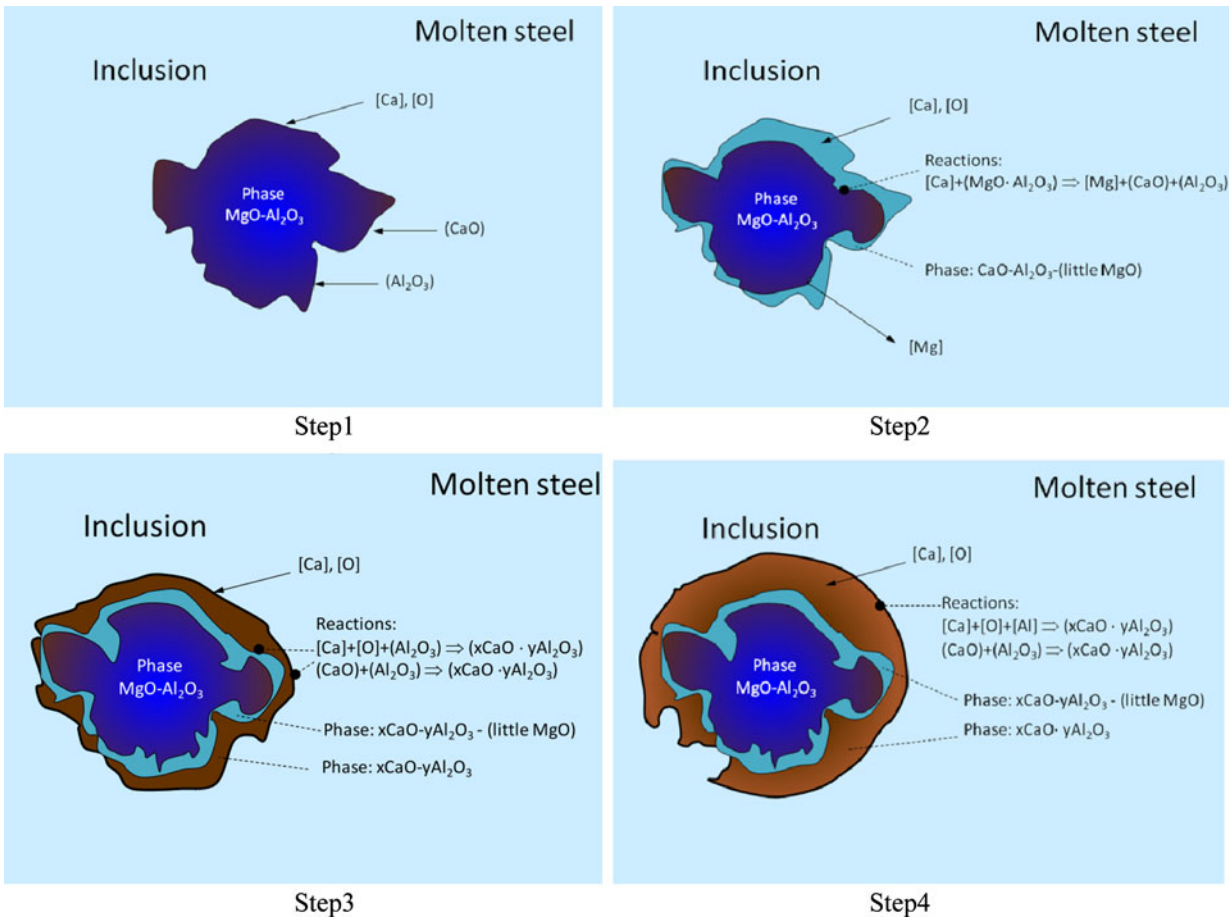

Fig. 15—Steps for the modification of MgO-Al_2O_3 inclusions.

During this step, Reaction [15] dominates the modification process. [Ca] and [Al] are the dissolved calcium and aluminum in the molten steel. In the current industrial trial, 300 kg aluminum wire was added into the molten steel before calcium treatment, and 60 kg aluminum wire was added into the steel after the calcium treatment. So, the concentration of the dissolved aluminum will be high enough for these reactions. (Al_2O_3) can be the newly precipitated inclusions or the inclusions that has been in the molten steel.

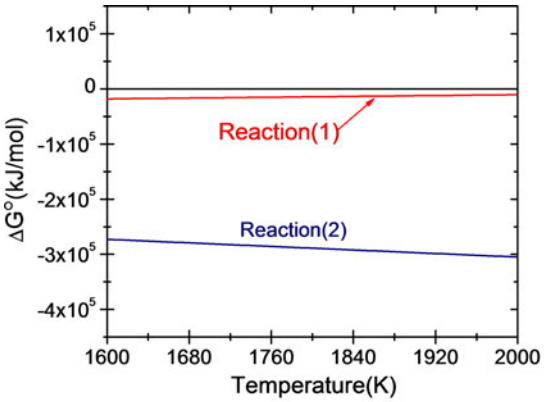

Reaction (1):

$$[Ca] + (MgO) = (CaO)\cdot + [Mg] \quad \Delta G = 18.92T - 48249 \ [12]$$

Reaction (2):

$$[Ca] + [O] + 7/12(Al_2O_3) = (CaO)\cdot 7/12(Al_2O_3) \quad \Delta G = -80.32T - 144291 \ [12,49]$$

Fig. 16—Comparison of the standard Gibbs energy for two reactions.

Step 2: Generating liquid $xCaO\cdot yAl_2O_3$ layer at the outside of the spinel inclusion.

When the thin layer of $xCaO\cdot yAl_2O_3$ at the outside of the spinel inclusion becomes thicker and thicker, the diffusion of the replaced [Mg] to the molten steel through this layer becomes very slow, then the Reactions [16] through [19] will dominate the modification process. These reactions precipitate a layer of ($xCaO\cdot yAl_2O_3$) at the outside of the spinel inclusion. If ($xCaO\cdot yAl_2O_3$) is liquid, for example ($12CaO\cdot 7Al_2O_3$), then this outside ($xCaO\cdot yAl_2O_3$) will cover the original irregular shape spinel and become a spherical shape because of the surface tension of the liquid ($xCaO\cdot yAl_2O_3$) phase. The thickness of the outer ($xCaO\cdot yAl_2O_3$) layer is approximately the quarter of the diameter of the final inclusion.

If Reaction [15] proceeds longer time, then the $MgO\cdot Al_2O_3$ core will become spherical, like the inclusions shown in Figures 1(b) and 2(b). If this reaction can only proceed a short time or the generation of the $xCaO\cdot yAl_2O_3$ layer by Reactions [18] and [19] is very quick, then the reducing of MgO by the dissolved calcium is very slow and the $MgO\cdot Al_2O_3$ core will keep their original irregular shape (as shown in Figures 1(a), (b), (d), (e), 9(c), and 14).

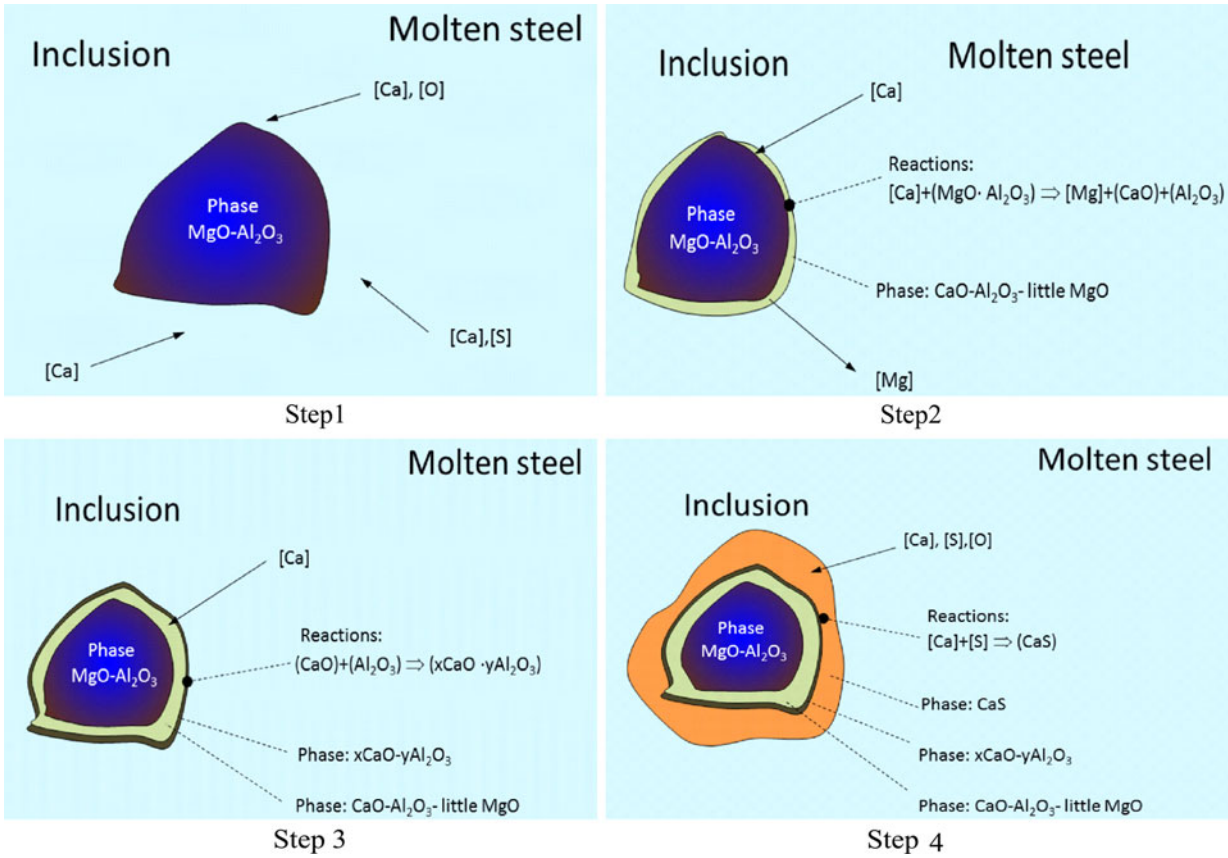

Fig. 17—Modification mechanism of a $MgO\text{-}Al_2O_3$ inclusion into a $MgO\text{-}Al_2O_3$–CaO-CaS inclusion.

Figure 16 indicates that thermodynamically Reaction [18] is easier to occur than Reaction [15].

Step 3: Generating solid CaS-CaO layer at the outside of the spinel inclusion if the local sulfur is higher.

If the local sulfur in the molten steel is high enough, then Reaction [21] will occur. Or, during cooling and solidification process the precipitated sulfur and the dissolved calcium will react, and generate CaS inclusions. These CaS inclusions will precipitate at the surface of $MgO{\cdot}Al_2O_3$ inclusions. Since CaS is solid at the temperature of the molten steel, so it will change the irregular shape of the $MgO{\cdot}Al_2O_3$ inclusion. Thus, no modification effect can be seen for this kind of mechanism. The schematic in Figure 17 summarized this kind of mechanism, and the example for this kind of modification mechanism is shown in Figure 8.

$$[Ca] + [S] = (CaS) \qquad [21]$$

Therefore, the calcium treatment does not fully modify the $MgO{\cdot}Al_2O_3$ inclusions into uniform $CaO\text{-}MgO\text{-}Al_2O_3$ inclusions or $CaO\text{-}Al_2O_3$ inclusions rather than partially replace the MgO in the inclusion into the dissolved Mg and enters the molten steel. In addition, the treatment covers a new liquid layer of $xCaO{\cdot}yAl_2O_3$ at the outside of the inclusion. Thus, the size of the $MgO{\cdot}Al_2O_3$ inclusions after the calcium treatment should be larger than that before calcium, which has been proven in Figure 6. Thus, the core of the spinel inclusions will be a pure $MgO{\cdot}Al_2O_3$ phase no matter with and without calcium treatment because the core of the spinel inclusion does not join any of the reactions. This has been proven by Figures 1, 9, 10, 14, and 15. It has to be mentioned that although the inclusions shown in Figures 1, 9, 10, 14, and 15 have the pure $MgO\text{-}Al_2O_3$ core inside, the EDX area scanning may locate these inclusions in the liquid region of $CaO\text{-}MgO\text{-}Al_2O_3$ diagram under 1873 K (1600 °C), as shown in Figure 4. The reason that the two inclusions shown in Figure 12 had different Al_2O_3 at the outside layer is that more Reactions of [16] through [19] occurred for the inclusion shown in Figure 12(b) than Figure 12(a).

It is known that $MgO{\cdot}Al_2O_3$ spinel inclusions have detrimental effect on the rolling process because of their high melting point (2408 K [2135 °C]) and high hardness (HV = 2100 to 2400 kg/mm^2). Because $MgO{\cdot}Al_2O_3$ inclusions are solid at the temperature of the molten steel, the core of the spinel inclusions is always solid no matter with and without calcium treatment. So, this kind of modification has no help on the shape control of $MgO{\cdot}Al_2O_3$ inclusions during subsequent rolling processes. Figure 18 shows the deformation of these kinds of inclusions during rolling, where the $MgO{\cdot}Al_2O_3$ core will keep its original shape.

Thus, attentions should be paid on the diminishing the generation and improving the removal of $MgO{\cdot}Al_2O_3$ inclusions rather than modifying it using calcium treatment.

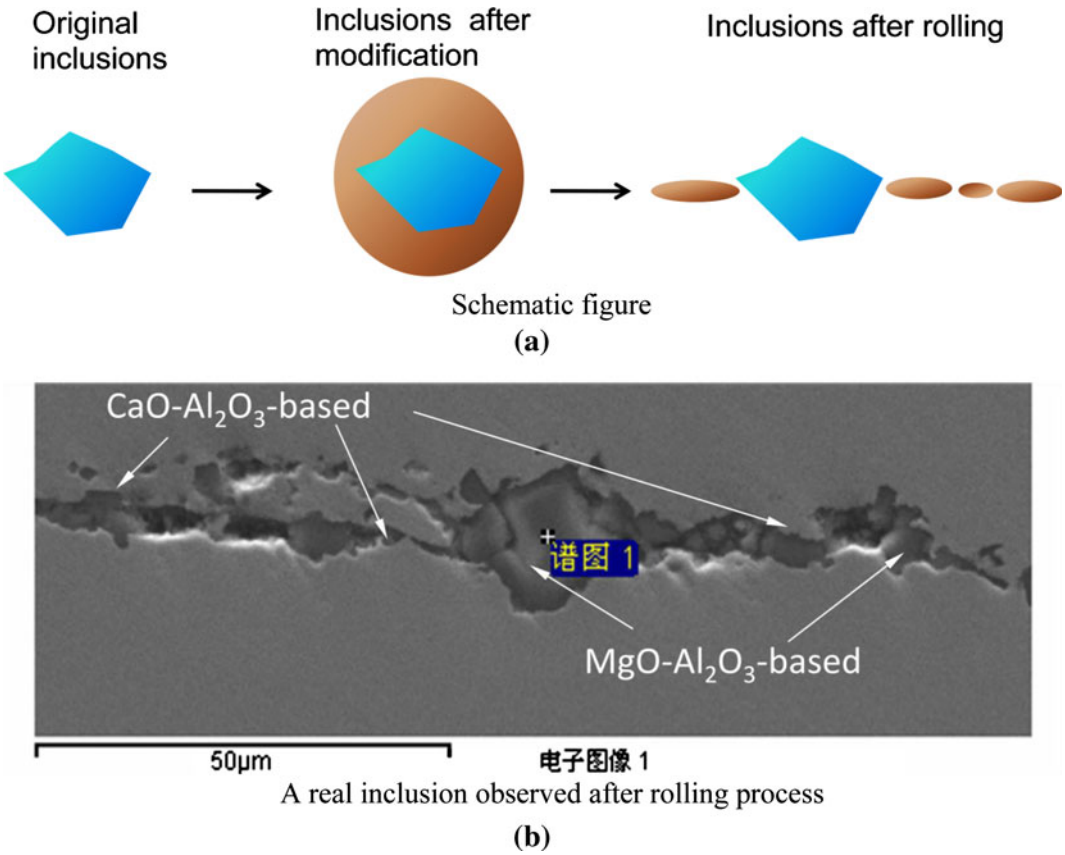

Fig. 18—Deformation of the inclusion with $MgO\text{-}Al_2O_3$ core during rolling: (*a*) schematic figure and (*b*) a real inclusion observed after rolling process.

The current conclusion is different from other researchers who reported that all of the MgO can be reduced into the dissolved Magnesium and then $MgO{\cdot}Al_2O_3$ inclusion is modified into spherical CaO-Al_2O_3 inclusion, or to a uniform CaO-MgO-Al_2O_3 inclusion. The current study hardly observed the uniform liquid CaO-MgO-Al_2O_3 phase across the entire cross section of the spinel inclusion in the steel after calcium treatment.

The authors also agree that under the following conditions, Reaction [15] will dominate the modification of $MgO{\cdot}Al_2O_3$ inclusion, and these inclusions can be fully modified: (1) a situation in which the kinetic condition for the diffusion of the dissolved magnesium in the inclusions can be improved, (2) long enough refining time; and (3) small size of inclusions. As shown in Figures 1, 7, and 12, after calcium treatment, the $MgO{\cdot}Al_2O_3$ core is larger than 5 μm, and Figure 7(b) shows that the intermediate layer with more Al_2O_3 and less MgO and CaO was approximately 2 μm, which implies that the penetration depth of Reaction [15] is approximately 2 μm. Thus, it is rational to conclude that <2 μm $MgO{\cdot}Al_2O_3$ inclusions can be modified into CaO-Al_2O_3 inclusions by the reducing Reaction [15]; and for >5 μm $MgO{\cdot}Al_2O_3$ inclusions, MgO can only be partially modified into CaO-Al_2O_3 inclusions, and the resulting inclusions will have a $MgO{\cdot}Al_2O_3$ core and an outside liquid CaO-Al_2O_3 layer.

VIII. CONCLUSIONS

The current study performed thermodynamic calculation, laboratory experiments, and industrial trials for the formation and modification of MgO-Al_2O_3 spinel inclusions in 30CrMo steel alloy steels. The following conclusions were obtained:

1. The stability Mg-Al-O diagram was obtained using thermodymanic study. For the current alloy steel, $MgO{\cdot}Al_2O_3$ inclusions can form.
2. The MgO-Al_2O_3-CaO inclusions were regular in shape and smaller than 3 μm before calcium treatment and mainly 2 to 5 μm after calcium treatment. The composition distribution of >5 μm inclusions after calcium treatment is inhomogeneous and has a two-layer structure: outside CaO-Al_2O_3 layer and MgO-Al_2O_3 core, and MgO and CaO can hardly coexist at the same location. The diffusion of Mg in the calcium aluminate layer may be the control step for the modification of $MgO{\cdot}Al_2O_3$ by Ca treatment. The CaO of the inclusions after calcium treatment was not from the replacing reaction between the dissolved [Ca] in the molten steel and the (MgO) in the inclusion, but it stemed from the reaction between [Ca] and [O] or (CaO) with (Al_2O_3).
3. The modification of >5 μm $MgO{\cdot}Al_2O_3$ spinel inclusions by calcium treatment includes two steps: (1) replacing MgO in the inclusion by the dissolved calcium in the steel and (2) generating a liquid $xCaO{\cdot}yAl_2O_3$ layer at the outside of the spinel inclusion. Therefore, the calcium treatment can hardly fully modify the $MgO{\cdot}Al_2O_3$ inclusions, but can replace part of MgO in the inclusion into the dissolved Mg and cover a new liquid layer of $xCaO{\cdot}yAl_2O_3$ at the outside of the inclusion. This kind of modification will have little help on the shape control of the $MgO{\cdot}Al_2O_3$ inclusions during a subsequent rolling process because the core of the inclusion is still pure $MgO{\cdot}Al_2O_3$ spinel. Attention should be paid on diminishing the generation and improving the removal of $MgO{\cdot}Al_2O_3$ inclusions rather than on modifying them using calcium treatment.
4. $MgO{\cdot}Al_2O_3$ inclusions can be fully modified into $CaO{\cdot}Al_2O_3$ if the kinetic condition for the diffusion of the dissolved magnesium in the inclusions can be improved, the refining time can be long enough, and inclusions are smaller than 2 μm. $MgO{\cdot}Al_2O_3$ inclusions with size of <2 μm can be fully modified into CaO-Al_2O_3 inclusions by the reducing reaction between (MgO) in the inclusion and the dissolved [Ca] in the steel.

ACKNOWLEDGMENTS

This research is supported by the Laboratory of Green Process Metallurgy and Modeling (GPMM), the High Quality Steel Consortium, the School of Metallurgical and Ecological Engineering at University of Science and Technology Beijing (USTB), and the National Science Foundation of China (No.51074021).

REFERENCES

1. S. Inada and H. Todoroki: *Technology for Control of Nonmetallic Inclusions and Production of Clean Steels*, No. 182 and 183 Nishiyama Memorial Seminar, The Iron and Steel Institute of Japan, Kyoto, Japan, 2004, p. 227.
2. J.H. Park and H. Todoroki: *ISIJ Int.*, 2010, vol. 50 (10), pp. 1333–46.
3. K. Sakata: *ISIJ Int.*, 2006, vol. 46 (12), pp. 1795–99.
4. Y. Wang, X. Zuo, and L. Zhang: *The Seventh Int. Conf. of Clean Steel*, Balatonfüred, Hungary, 2007, pp. 161–72.
5. S. Liu, X. Wang, X. Zuo, Y. Wang, L. Zhang, S. Niu, M. Liang, and C. Li: *Rev, Metall.-Paris*, 2008, vol. 105 (2), pp. 72–79.
6. J. Gao, M. Long, Y. Wang, X. Zuo, and L. Zhang: *Mater. Sci. Technol.*, 2009, pp. 1054–67.
7. S. Wu, Y. Wang, L. Zhang, and J. Zhang: *Proc. of AISTech 2009 Iron & Steel Technol. Conf. and Exposition*, Vol. II, AIST, St. Louis, MO, 2009, pp. 543–58.
8. S. Li, X. Zuo, K. Peng, Y. Wang, and L. Zhang: *Proc. of AISTech 2009 Iron & Steel Technol. Conf. and Exposition*, Vol. II, St. Louis, MO, 2009, pp. 589–601.
9. X. Zuo, M. Long, J. Gao, Y. Wang, and L. Zhang: *Iron Steel Tech.*, 2010, vol. 7 (10), pp. 65–76.
10. S. Li, W. Jin, L. Zhang, X. Zuo, and Y. Wang: *Proc. of AISTech 2007 Iron & Steel Technol. Conf. and Exposition*, vol. I, AIST, Warrandale, PA, 2008, pp. 899–913.
11. H. Itoh, K. Fujii, T. Nagasaka, and M. Hino: *Steel Res.*, 2003, vol. 74, p. 86.
12. H. Itoh, M. Hino, and S. Ban-ya: *Metall. Mater. Trans. B*, 1997, vol. 28B, p. 953.
13. T.N.A.M.H.K. Fujii: *ISIJ Int.*, 2000, vol. 40, p. 1059.
14. W.G. Seo, W.H. Han, J.S. Kim, and J.J. Pak: *ISIJ Int.*, 2003, vol. 43 (2), pp. 201–08.

15. T. Nishi and K. Shinme: *Tetsu-to-Hagané*, 1998, vol. 84 (12), pp. 837–43.
16. G. Okuyama, K. Yamaguchi, S. Takeuchi, and K.-I. Sorimachi: *ISIJ Int*., 2000, vol. 40, p. 121.
17. V. Brabie: *Steel Res*., 1997, vol. 2, p. 54.
18. V. Brabie: *ISIJ Int*., 1996, vol. 36, pp. S109–S12.
19. J.H. Park: *Metall. Mater. Trans. B*, 2007, vol. 38B, p. 657.
20. J.H. Park: *Mater. Sci. Eng. A*, 2007, vol. 472, pp. 43–51.
21. J.H. Park and D.S. Kim: *Metall. Mater. Trans. B*, 2005, vol. 36B, pp. 495–502.
22. H. Itoh, M. Hino, and S. Ban-Ya: *Metall. Mater. Trans. B*, 1997, vol. 28B, pp. 953–56.
23. H. Itoh, M. Hino, and S. Ban-ya: *Tetsu-To-Hagané/J. Iron Steel Inst. Japan*, 1998, vol. 84 (2), pp. 85–90.
24. K. Fujii, T. Nagasaka, and M. Hino: *ISIJ Int*., 2000, vol. 40 (11), pp. 1059–66.
25. W.G. Seo, W.H. Han, J.S. Kim, and J.J. Pak: *ISIJ Int*., 2003, vol. 43 (2), pp. 201–08.
26. K. Mizuno, H. Todoroki, M. Noda, and T. Tohge: *Ironmaker Steelmaker*, 2001, vol. 28 (8), pp. 93–101.
27. H. Todoroki, K. Mizuno, and M. Noda: *Steelmaking Conf. Proc*, Warrendale, PA, 2001, pp. 331–41.
28. H. Todoroki and S. Inada: *Bull. ISIJ*, 2003, vol. 8, p. 575.
29. H. Todoroki and K. Mizuno: *ISIJ Int*., 2004, vol. 44 (8), pp. 1350–57.
30. G. Okuyama, K. Yamaguchi, S. Takeuchi, and K.I. Sorimachi: *ISIJ Int*., 2000, vol. 40 (2), pp. 121–28.
31. V. Brabie: *Steel Res*, 1997, vol. 68 (2), pp. 54–60.
32. G.J.W. Kor: *Proc. of 1st Int. Calcium Treatment Symp*., Glasgow, Scotland, 1988, p. 39.
33. B. Harkness and D. Dyson: *METEC Congr. 94 and 2nd Eur. Continuous Casting Conf*, VDEh, Duesseldorf, Germany, 1994, p. 70.
34. K. YoungJo, L. Fan, M. Kazuki, and S. Du: *Steel Res. Int*., 2006, vol. 77 (11), pp. 785–92.
35. P.C. Pistorius, P. Presoly, and K.G. Tshilombo: *Proc. of TMS Annual Meeting and Exhibition*, San Antonio, TX, 2006, pp. 373–78.
36. N. Verma, P.C. Pistorius, R.J. Fruehan, W. Noh, and M. Potter: *Proc. of Materials Science & Technology 2009 (MS&T'09)*, Pittsburgh, PA, 2009, vol. 2, pp. 1042–53.
37. N. Verma, P.C. Pistorius, and R.J. Fruehan: *Proc. of AISTech 2011 Iron & Steel Technology Conf. and Exposition*, vol. 2, Indianapolis, IN, 2011, pp. 607–15.
38. E.B. Pretorius, H.G. Oltmann, and T. Cash: *Proc. of AISTech 2009 Iron & Steel Technology Conf. and Exposition*, vol. 1, St. Louis, MO, 2009, pp. 1035–49.
39. M. Jiang, X. Wang, B. Chen, and W. Wang: *ISIJ Int*., 2008, vol. 48 (7), pp. 885–90.
40. X. Wang, H. Li, Y. Wang, K. Zhao, and T. Chen: *Proc. of AIS-Tech 2009 Iron & Steel Technology Conf. and Exposition*, vol. 1, St. Louis, MO, 2009, pp. 965–72.
41. M. Jiang, X. Wang, B. Chen, and W. Wang: *ISIJ Int*., 2010, vol. 50 (1), pp. 95–104.
42. M. Jiang, X.H. Wang, and W.J. Wang: *Steel Res. Int*., 2010, vol. 81 (9), pp. 759–65.
43. S.K. Michelic, M. Hartl, and C. Bernhard: *Proc. of AISTech 2011 Iron & Steel Technology Conf. and Exposition*, vol. 2, Indianapolis, IN, 2011, pp. 617–26.
44. J.H. Park, D.S. Kim, and S.B. Lee: *Metall. Mater. Trans. B*, 2005, vol. 36B, pp. 67–73.
45. A. Martín, E. Brandaleze, J. Madías, R. Donayo, A. Gómez, and J. Pérez: *Proc. of the 7th Int. Conf. of Clean Steel*, Balatonfüred, Hungary, 2007, pp. 203–11.
46. M. Jiang: Masters Thesis, University of Science and Technology Beijing, Beijing, China, 2009.
47. J.H. Park: *Metall. Mater. Trans. B*, 2007, vol. 38B, pp. 657–63.
48. J. Björklund, M. Andersson, and P. Jönsson: *Proc. of the 7th Int. Conf. of Clean Steel*, Balatonfüred, Hungary, 2007, pp. 212–21.
49. R.H. Rein and J. Chipman: *Metall. Soc. Am. Inst. Mining, Metall. Petrol. Engineer.–Trans*., 1965, vol. 233, p. 415.